8

Three-Dimensional Problems with Translational or Rotational Symmetry

The electromagnetic scattering formulations considered in preceding chapters have been limited to two-dimensional, infinite cylinder geometries. These two-dimensional formulations require both the scatterer and the excitation to be invariant along a preferred axis, which may not be a realistic model of the desired physical problem. A wider class of problems may be modeled under the assumption that, while the scatterer is translationally invariant along z, the source may vary with z or may be finite in extent. The fields of an arbitrary source may be decomposed into a spectrum of plane waves incident on the infinite cylinder from oblique angles with respect to z. The response to each plane wave can be obtained by the solution of a two-dimensional problem, after which the individual responses are superimposed to give the solution to the original three-dimensional problem. Because of their translational invariance, these three-dimensional problems impose computational requirements similar to two-dimensional problems. The "building block" in this analysis is the scattering of an obliquely incident wave from an infinite cylinder, and several formulations for oblique scattering will be described in this chapter.

Axisymmetric scatterers, sometimes known as *bodies of revolution*, permit a similar reduction in computational effort. As a function of the circumferential variable, the fields and currents can be represented by cylindrical harmonics that decouple the pertinent equations and reduce the effective dimensionality of the problem. Simple examples of the axisymmetric scattering problem are illustrated in Sections 8.7 and 8.8. Section 8.7 describes a surface integral equation formulation, while Section 8.8 presents a scalar differential equation formulation.

8.1 SCATTERING FROM INFINITE CYLINDERS ILLUMINATED BY FINITE SOURCES [1]

Consider a finite source radiating in the presence of an infinite, perfectly conducting cylinder, as depicted in Figure 8.1. Using the equivalence principle from Section 1.6, the scattered fields can be expressed in terms of the equivalent electric current density $\bar{J}$ located on the cylinder surface. Because the source is finite, the electromagnetic fields vary with all three spatial variables.

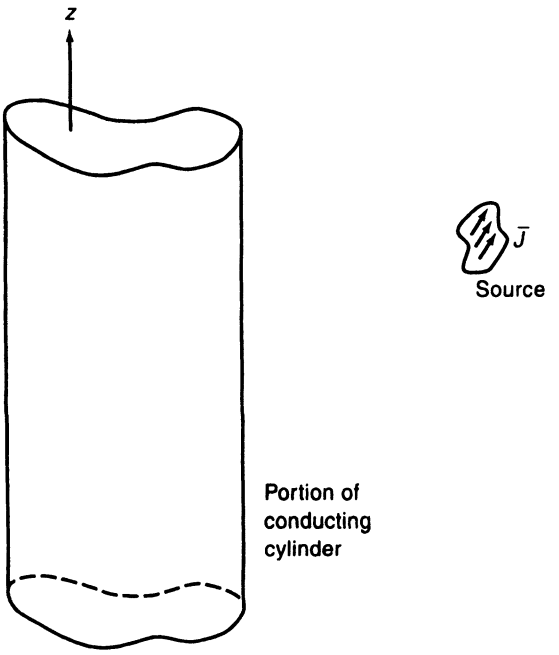

Figure 8.1 Conducting cylinder illuminated by a finite source.

Suppose the cylinder axis lies along $\hat{z}$, as illustrated in Figure 8.1. The *Fourier transform* with respect to z can be defined as

$$F_z\{A(z)\} = \tilde{A}(k_z) = \int_{-\infty}^{\infty} A(z)e^{-jk_z z}\,dz \tag{8.1}$$

This transformation converts functions of the spatial variable z to functions of the "spectral" variable k_z. If the Fourier transform is applied to all of the field quantities and equations describing the scattering problem, the solution for unknown surface current density can be obtained in the Fourier transform domain (sometimes called the spectral domain or *k-space*) as a function of k_z. Once the solution for $\bar{J}$ is obtained as a function of k_z, the *inverse Fourier transform*

$$F_z^{-1}\{\tilde{A}(k_z)\} = A(z) = \frac{1}{2\pi}\int_{-\infty}^{\infty} \tilde{A}(k_z)e^{jk_z z}\,dk_z \tag{8.2}$$

can be employed to return to the spatial domain.

The task of transforming the quantities into the Fourier transform domain would be of little use were it not for the following: As a consequence of the invariance of the cylinder geometry, the z-dependence of the wave equation can be separated in accordance with the classical separation-of-variables procedure. Because the kernel of the Fourier transform is a characteristic solution of the wave equation, the transformed equations are uncoupled as a function of k_z. In other words, the solution for the transform of $\tilde{J}$ can be obtained at one value of k_z by the solution of a two-dimensional equation without regard for the solution at other values of k_z.

For example, suppose that an infinite conducting cylinder is analyzed using the three-dimensional MFIE. The $\hat{z}$-component of the MFIE only involves the transverse current density and can be expressed in the spatial domain as

$$H_z^{\text{inc}}(t, z) = -J_t(t, z) - \hat{z} \cdot \nabla \times \iint \hat{t}(t') J_t(t', z') \frac{e^{-jkR}}{4\pi R} \, dt' \, dz' \tag{8.3}$$

where

$$R = \sqrt{[x(t) - x(t')]^2 + [y(t) - y(t')]^2 + (z - z')^2} \tag{8.4}$$

and the integration is assumed to be restricted to the surface of a closed mathematical cylinder whose cross-sectional shape is defined parametrically by the variable t. Equation (8.3) involves a convolution in the variable z, and an application of the Fourier transform in conjunction with the convolution theorem

$$F_z\{A(z) * B(z)\} = \tilde{A}(k_z)\tilde{B}(k_z) \tag{8.5}$$

produces the transformed equation

$$\tilde{H}_z^{\text{inc}}(t, k_z) = -\tilde{J}_t(t, k_z) - \hat{z} \cdot \nabla \times \int \hat{t}(t') \tilde{J}_t(t', k_z) \tilde{G}(\rho; k, k_z) \, dt' \tag{8.6}$$

where

$$\tilde{G}(\rho; k, k_z) = F_z\left\{\frac{e^{-jk\sqrt{\rho^2+z^2}}}{4\pi\sqrt{\rho^2+z^2}}\right\} = \begin{cases} \dfrac{1}{4j} H_0^{(2)}\left(\rho\sqrt{k^2 - k_z^2}\right) & k^2 > k_z^2 \\ \dfrac{1}{2\pi} K_0\left(\rho\sqrt{k_z^2 - k^2}\right) & k_z^2 > k^2 \end{cases} \tag{8.7}$$

$$\rho = \sqrt{[x(t) - x(t')]^2 + [y(t) - y(t')]^2} \tag{8.8}$$

and $H_0^{(2)}$ and K_0 represent the Hankel and modified Bessel functions of the second kind, respectively. The Fourier transform in Equation (8.7) has effectively produced the two-dimensional free-space Green's function from Equation (1.47) with the wavenumber in the argument replaced by the transverse wavenumber

$$k_t = \begin{cases} \sqrt{k^2 - k_z^2} & k^2 > k_z^2 \\ -j\sqrt{k_z^2 - k^2} & k_z^2 > k^2 \end{cases} \tag{8.9}$$

This result can also be obtained from a direct application of the Fourier transform to the Helmholtz equation (Prob. P8.1). In the Fourier transform domain, the equation to be solved at each value of k_z is essentially the two-dimensional MFIE discussed in Section 2.2, with the wavenumber in the argument replaced by the transverse wavenumber of (8.9). An electromagnetic wave propagating at an oblique angle with respect to the cylinder

axis involves the identical transverse wavenumber and suggests the interpretation that the Fourier transform decomposes the field into a spectrum of waves incident from oblique spatial angles.

The original three-dimensional problem of a finite source radiating in the presence of an infinite cylinder involves three coupled spatial variables x, y, and z. If cast into the Fourier transform domain, the solution as a function of k_z can be obtained by solving uncoupled two-dimensional equations involving the variables x and y and the parameter k_z. Consequently, this approach is much more amenable to numerical solution than the original three-dimensional problem. However, we are still faced with the task of solving the two-dimensional equations over the infinite continuum spanned by the variable k_z in order to construct the inverse transformation according to (8.2).

A numerical implementation of the inverse Fourier transform requires that the continuum spanned by k_z be truncated and discretized. In other words, we construct the solution at a finite number of values $\{k_{zi}\}$, where i may range from $-N$ to N. Assuming evenly spaced samples as a function of k_z, the inverse Fourier transform is approximated by

$$A(z) \cong \frac{\Delta k_z}{2\pi} \sum_{n=-N}^{N} \tilde{A}(n\ \Delta k_z) e^{jnz\,\Delta k_z} \tag{8.10}$$

If desired, this summation could be implemented with the aid of a fast Fourier transform (FFT) algorithm. As is well known from signal analysis, the combination of an evenly spaced sampling procedure with a Fourier transform is equivalent to working directly with the Fourier transform of a periodic extension of the original function of z. Thus, the approximations inherent in Equation (8.10) are equivalent to replacing the original finite source with an infinite, periodic array of sources distributed along the axis of the cylinder. The period of this fictitious array is related to the sampling interval Δk_z by

$$P_z = \frac{2\pi}{\Delta k_z} \tag{8.11}$$

To successfully employ the procedure, the equivalent spatial period P_z must be sufficiently large so that the contribution of the fictitious sources to the currents on the cylinder is negligible in the region of interest compared with the contribution of the desired source. In addition, the truncation of the spectrum as a function of k_z must not introduce inaccuracy. We observe that it will generally be necessary to consider both the *visible region* of the spectrum ($k_z < k$) and the *invisible region* ($k_z > k$). (Wave propagation in the transverse direction is evanescent in the invisible region.) For most problems, it will be necessary to analyze a large number of two-dimensional problems before inverse transformation. The specific number will depend on the actual source distribution.

Note that scanning the transverse wavenumber over a range of values is equivalent to varying the electrical size of the scatterer or the frequency under consideration. Therefore, it is likely that "interior resonance" frequencies discussed in Chapter 6 will be encountered throughout the range necessary for inverse transformation. It is therefore essential to employ the alternative formulations described in Chapter 6 to ensure a robust formulation, at least throughout the visible region of the spectrum.

The following sections present several different approaches for treating the scattering of an oblique wave from conducting or penetrable cylinders. While these formulations provide a complete model for a single incident wave, they also constitute the basic building block required for the analysis of a finite source radiating in the presence of an infinite cylinder.

8.2 OBLIQUE TM-WAVE SCATTERING FROM INFINITE CONDUCTING CYLINDERS: CFIE DISCRETIZED WITH PULSE BASIS FUNCTIONS AND DELTA TESTING FUNCTIONS

Consider an infinite, perfectly conducting cylinder illuminated by a uniform plane wave incident from an oblique angle with respect to the cylinder axis (Figure 8.1). For a TM uniform plane wave, the z-component of the incident electric field has the form

$$E_z^{\text{inc}}(x, y, z) = e^{-jk_t(x\cos\theta + y\sin\theta)} e^{jk_z z} \tag{8.12}$$

The surface equivalence principle can be employed to replace the conducting material by equivalent electric currents J_z. In order to ensure unique solutions at all frequencies, we consider a numerical solution of the CFIE. Equation (6.12) can be generalized for an oblique excitation by replacing the wavenumber k by the transverse wavenumber k_t defined in (8.9), to produce

$$\begin{aligned} \alpha E_z^{\text{inc}}(t) + (1-\alpha)\eta H_t^{\text{inc}}(t) = (1-\alpha)\eta J_z(t) + j\alpha\eta\frac{k_t^2}{k}\int J_z(t')\tilde{G}(\rho; k, k_z)\, dt' \\ -(1-\alpha)\eta\hat{t}\cdot\nabla\times\int \hat{z}J_z(t')\tilde{G}(\rho; k, k_z)\, dt' \end{aligned} \tag{8.13}$$

where $\tilde{G}$ is defined in Equation (8.7). Although this CFIE remains valid if k_t is purely imaginary, which would occur if $k_z > k$, there are no "interior resonance" frequencies with $k_z > k$, and consequently the conventional EFIE or MFIE alone would be a more efficient choice throughout the invisible region of the spectrum.

Following the approach of Section 6.2, the CFIE can be discretized using pulse basis functions and Dirac delta testing functions to produce a matrix equation

$$\begin{bmatrix} C_{11} & C_{12} & \cdots & C_{1N} \\ C_{21} & C_{22} & \ddots & \vdots \\ \vdots & & & \\ C_{N1} & \cdots & \cdots & C_{NN} \end{bmatrix} \begin{bmatrix} j_1 \\ j_2 \\ \vdots \\ j_N \end{bmatrix} = \begin{bmatrix} e_1 \\ e_2 \\ \vdots \\ e_N \end{bmatrix} \tag{8.14}$$

Using the conventions for normal and tangent vectors from Figure 6.6 and Equations (6.19) and (6.20), the diagonal and off-diagonal entries are

$$C_{mm} = \frac{(1-\alpha)\eta}{2} + \frac{\alpha\eta k_t^2}{4k}\int_{\text{cell}\,m} H_0^{(2)}(k_t R_m)\, dt' \tag{8.15}$$

and

$$C_{mn} = \frac{\alpha\eta k_t^2}{4k}\int_{\text{cell }n} H_0^{(2)}(k_t R_m)\,dt' + \frac{(1-\alpha)\eta j k_t}{4}\int_{\text{cell }n}\left[\sin\Omega_m\left(\frac{y_m - y'}{R_m}\right) + \cos\Omega_m\left(\frac{x_m - x'}{R_m}\right)\right] H_1^{(2)}(k_t R_m)\,dt' \tag{8.16}$$

respectively, where

$$R_m = \sqrt{[x_m - x(t')]^2 + [y_m - y(t')]^2} \tag{8.17}$$

If the incident field is given by Equation (8.12), the entries of the excitation column vector are

$$e_m = \left[\alpha - (1-\alpha)\frac{k^2}{k_t^2}\cos(\theta - \Omega_m)\right] e^{-jk_t(x_m\cos\theta + y_m\sin\theta)} \tag{8.18}$$

These expressions involve integrals that are identical in form to those of the EFIE and MFIE discussed in Chapter 2, and their numerical evaluation is similar. As discussed in Chapter 6, the computational effort required to construct the CFIE matrix equation is roughly double that required for the EFIE or MFIE alone.

For illustration, Figure 8.2 shows the current density induced on an ogival cylinder by a plane wave incident at an angle 45° from normal using the CFIE formulation. Table 8.1 provides the bistatic scattering cross section for several discretizations of the same geometry, defined for the oblique TM case as

$$\sigma_{\text{TM}}(\phi) = \lim_{\rho\to\infty} 2\pi\rho\frac{|E_z^s(\rho,\phi)|^2}{|E_z^{\text{inc}}(0,0)|^2} \tag{8.19}$$

These results were obtained using a weighting parameter $\alpha = 0.2$ within the CFIE (the selection of α has been discussed in Chapter 6).

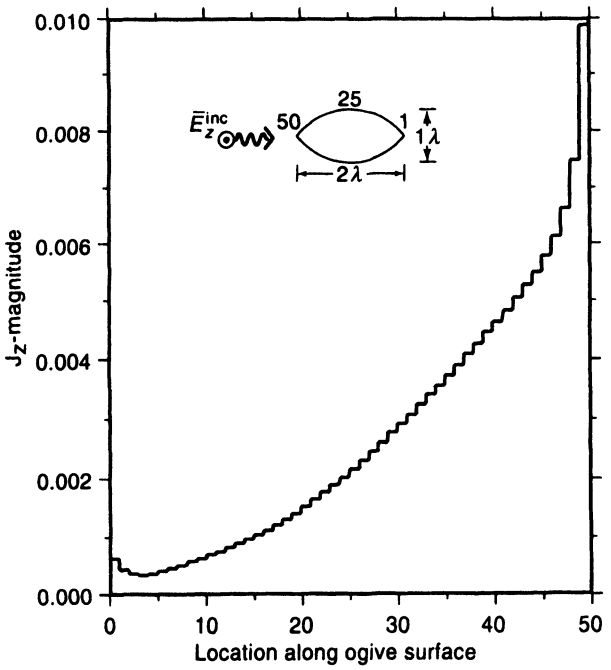

Figure 8.2 The CFIE result for the current density induced by an obliquely incident wave on an ogival p.e.c. cylinder. The incident field has unit magnitude E_z and impinges on the cylinder at an angle 45° from the x–y plane. The result was obtained using 100 pulse basis functions to represent J_z.

TABLE 8.1 Bistatic Two-Dimensional Scattering Cross Section (dB λ) for an Ogival Cylinder of Overall Dimension 2.0λ by 1.0λ Obtained Using the CFIE Formulation

ϕ (deg)	50-Cell Model	100-Cell Model	200-Cell Model
0	9.98	10.18	10.30
30	6.61	6.80	6.91
60	3.25	3.43	3.53
90	2.14	2.29	2.37
120	0.07	0.34	0.50
150	−1.28	−1.26	−1.24
180	−1.78	−1.86	−1.88

Note: The incident plane wave is TM to z and is incident at an angle that is 45° from the transverse plane and edge-on in the transverse plane. The 200-cell model represents a density of 43 cells per wavelength.

The CFIE formulation can easily be adapted to treat the TE polarization, and we leave that exercise to the reader (Prob P8.4). We note that the CFIE approach is just one of several integral equation formulations that eliminate the interior resonance difficulties. In the following section, we describe another procedure for oblique scattering from conducting cylinders: the augmented-field formulation. The augmented-field equations also eliminate spurious interior resonances.

8.3 OBLIQUE TE-WAVE SCATTERING FROM INFINITE CONDUCTING CYLINDERS: AUGMENTED MFIE DISCRETIZED WITH PULSE BASIS FUNCTIONS AND DELTA TESTING FUNCTIONS

A closed, perfectly conducting cylinder illuminated by an obliquely incident wave can also be analyzed using the augmented MFIE introduced in Section 6.4, and we turn our attention to that approach. The augmented-field formulation imposes boundary conditions on both the normal and tangential fields at the scatterer surface and, like the CFIE, guarantees unique solutions at all frequencies [2]. If the infinite conducting cylinder of Figure 8.1 is illuminated by an oblique TE wave having $\hat{z}$-component

$$H_z^{\text{inc}}(x, y, z) = e^{-jk_t(x\cos\theta + y\sin\theta)} e^{jk_z z} \tag{8.20}$$

both $\hat{z}$- and $\hat{t}$-components of $\bar{J}$ are excited. Although the $\hat{z}$-component of the MFIE only couples to the transverse current density, even in the case of oblique excitation, both the CFIE and the augmented MFIE formulations couple to both $\hat{z}$- and $\hat{t}$-components of the current density and consequently require twice the number of unknowns in this situation to ensure unique solutions at all frequencies. The augmented MFIE formulation offers the advantage that the matrix entries are simpler in form than those of the CFIE formulation

but at the same time imposes the disadvantage of working with all three components of the $\bar{H}$-field equation. As a result, the augmented-field formulation produces an overdetermined system of equations and requires additional storage and a more sophisticated matrix solution algorithm.

The augmented-field equations, constructed using the boundary conditions $\hat{n} \times \bar{H} = \bar{J}$ and $\hat{n} \cdot \bar{H} = 0$ at the surface of the conducting cylinder, have the form

$$H_z^{\text{inc}}(t) = -J_t(t) - \hat{z} \cdot \nabla \times \int \hat{t}(t') J_t(t') \frac{1}{4j} H_0^{(2)}(k_t R)\, dt' \tag{8.21}$$

$$H_t^{\text{inc}}(t) = J_z(t) - \hat{t} \cdot \nabla \times \int [\hat{t}(t') J_t(t') + \hat{z} J_z(t')] \frac{1}{4j} H_0^{(2)}(k_t R)\, dt' \tag{8.22}$$

$$H_n^{\text{inc}}(t) = -\hat{n} \cdot \nabla \times \int [\hat{t}(t') J_t(t') + \hat{z} J_z(t')] \frac{1}{4j} H_0^{(2)}(k_t R)\, dt' \tag{8.23}$$

where R and k_t have been defined in the preceding section. (For the special case of a normally incident TE wave, $H_t = 0$ and $H_n = 0$. In that case, this particular formulation reduces to the tangential-field MFIE and will not necessarily guarantee unique solutions.)

Assuming that the cylinder contour is represented in terms of flat strips as depicted in Figure 6.5, pulse basis functions can be used to represent both components of the current density. It is sufficient to enforce the resulting equations by point matching in the center of each cell in the model (following an approach similar to that used in Section 2.2 for normally incident TE waves). The resulting system of equations is overdetermined and can be written as

$$\begin{bmatrix} \mathbf{A} & \mathbf{0} \\ \mathbf{B} & \mathbf{C} \\ \mathbf{D} & \mathbf{E} \end{bmatrix} \begin{bmatrix} j_t \\ j_z \end{bmatrix} = \begin{bmatrix} H_z^{\text{inc}} \\ H_t^{\text{inc}} \\ H_n^{\text{inc}} \end{bmatrix} \tag{8.24}$$

The entries of (8.24) are given by

$$A_{mm} = -\tfrac{1}{2} \tag{8.25}$$

$$A_{mn} = -\int_{\text{cell } n} \left(\cos \Omega_n \frac{\partial \tilde{G}}{\partial x} + \sin \Omega_n \frac{\partial \tilde{G}}{\partial y} \right) dt' \qquad (m \neq n) \tag{8.26}$$

$$B_{mn} = -jk_z \sin(\Omega_m - \Omega_n) \int_{\text{cell } n} \tilde{G}(R_m; k, k_z)\, dt' \tag{8.27}$$

$$C_{mm} = \tfrac{1}{2} \tag{8.28}$$

$$C_{mn} = \int_{\text{cell } n} \left(\cos \Omega_m \frac{\partial \tilde{G}}{\partial x} + \sin \Omega_m \frac{\partial \tilde{G}}{\partial y} \right) dt' \qquad (m \neq n) \tag{8.29}$$

$$D_{mn} = jk_z \cos(\Omega_m - \Omega_n) \int_{\text{cell } n} \tilde{G}(R_m; k, k_z)\, dt' \tag{8.30}$$

and

$$E_{mn} = \int_{\text{cell}\,n} \left(\sin \Omega_m \frac{\partial \tilde{G}}{\partial x} - \cos \Omega_m \frac{\partial \tilde{G}}{\partial y} \right) dt' \tag{8.31}$$

In these expressions, $\tilde{G}(R_m; k, k_z)$ is defined in Equation (8.7) and R_m is defined in (8.17). Although these matrix elements are simpler in form than those produced by a CFIE formulation, the augmented MFIE approach involves additional overhead associated with the solution of the overdetermined $3N \times 2N$ system in Equation (8.24).

To illustrate the augmented MFIE formulation, consider a TE wave incident on a circular cylinder with three wavelength circumference at an oblique angle 36.75° from the normal. The tangential-field MFIE result for the transverse current density is shown in Figure 8.3. This particular oblique angle happens to correspond to an interior resonance, and as a result the MFIE result contains significant error. The augmented-field MFIE result is shown in Figure 8.4 and exhibits good agreement with the exact eigenfunction solution.

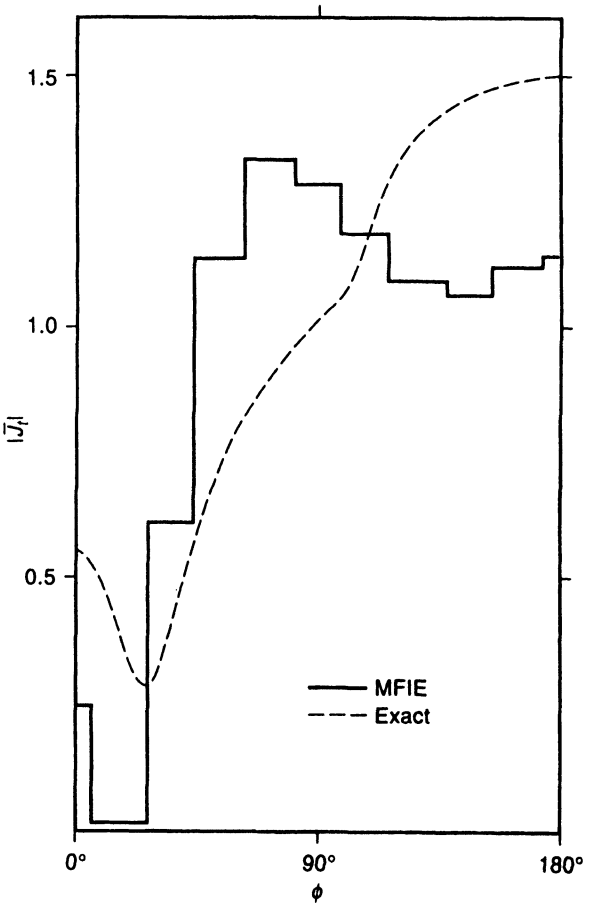

Figure 8.3 Tangential-field MFIE result for a circular cylinder with $ka = 3$ at an oblique angle $\theta^{\text{inc}} = 36.75°$.

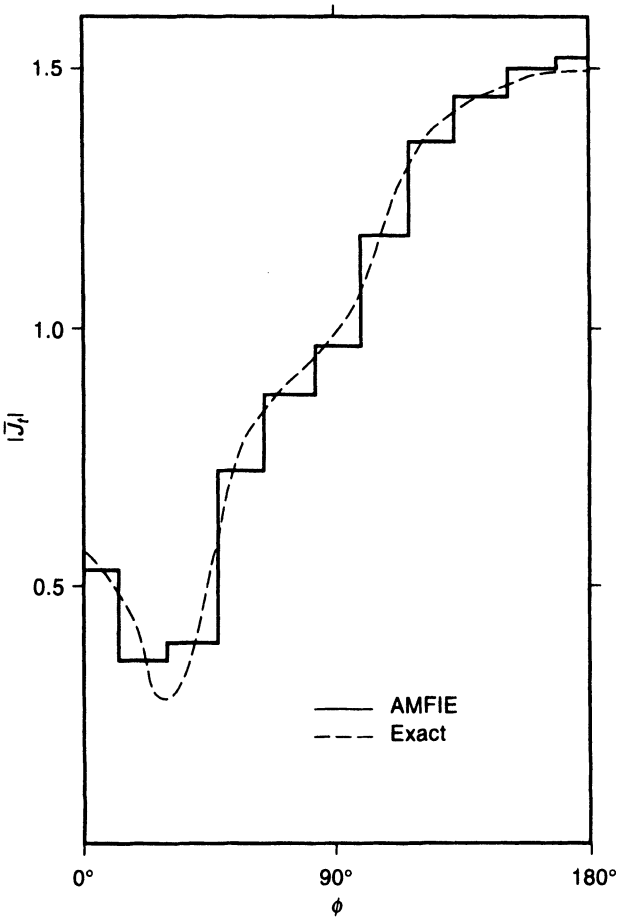

Figure 8.4 Augmented-field MFIE result for the problem in Figure 8.3.

8.4 APPLICATION: MUTUAL ADMITTANCE BETWEEN SLOT ANTENNAS [1]

To illustrate an application involving finite sources illuminating an infinite cylinder, consider the coupling between two slot antennas located on a conducting cylinder. The mutual admittance between two slots can be defined in accordance with Richmond's reaction theorem [3] and requires knowledge of the electric currents produced on a closed cylinder (at the location of aperture 2) by the source slot (aperture 1). Assuming that the tangential electric field in aperture 1 is known, an equivalent magnetic current density can be defined exterior to aperture 1 and used to generate the "incident" electric and magnetic fields in the vicinity of the cylinder as a function of the spectral variable k_z. In other words, using the Fourier transform from (8.1), the field produced by slot 1 is decomposed into a spectrum of waves incident upon the cylinder from oblique angles. Surface integral equation formulations similar to those described in Sections 8.2 and 8.3 can be used to produce the current

distribution induced by each incident wave. The currents can be superimposed according to the inverse Fourier transform in Equation (8.2) to yield the total current density needed for the mutual admittance calculation.

Reference [1] describes the details of the calculation and presents a variety of numerical results for coupling between two axial slots and two circumferential slots. (For axial slots the formulation requires the treatment of the TE polarization; for circumferential slots a combination of the TM and TE polarizations is required. Therefore, the actual approach differs slightly from the purely TM and TE situations discussed in Sections 8.2 and 8.3.) For illustration, Table 8.2 presents admittance data for axial slots in a circular cylinder as a function of the displacement along the cylinder axis. For this circular cylinder example, the numerical solutions exhibit good agreement with analytical values obtained using a cylindrical eigenfunction expansion [4]. Of course, the formulation is equally applicable to arbitrarily shaped cylinders.

TABLE 8.2 Mutual Admittance between Axial Slots in Circular Cylinder of Radius 1.0λ

Separation, Δz	Numerical Result		Eigenfunction Solution [4]	
	Magnitude (dB)	Angle (deg)	Magnitude (dB)	Angle (deg)
1λ	−86.22	−168.6	−87.1	−171
2λ	−99.13	−174.3	−100.0	−174
4λ	−111.66	−174.9	−112.4	−175
8λ	−124.32	−151.0	−124.3	−174

Note: The slots have height of 0.214λ and width of 0.5λ. Sampling imposes a fictitious spatial period P_z equal to 40.5λ; the spectrum included in the inverse Fourier transformation is truncated at $k_z = 20$. The cylinder is modeled with 88 equal-sized cells for moment-method analysis based on a CFIE formulation with pulse basis functions and Dirac delta testing functions [1].

The slot coupling example provides insight into the range of some of the parameters involved in the Fourier transformation process. In the actual implementation used in reference [1], the Fourier transform of the mutual admittance function $Y(z)$ was computed directly at each value of k_z as $\tilde{Y}(k_z)$, then transformed back to the spatial domain. Figures 8.5 and 8.6 show $\tilde{Y}(k_z)$ for circumferential and axial slots, respectively, and demonstrate that the support of the transform quantity is bandlimited to approximately 4 or 5 times the size of the visible region ($k_z \leq 2\pi$). Results from reference [1] also suggest that the fictitious period defined in Equation (8.11) must be at least 5 times the slot spacing to ensure reasonable accuracy for closely spaced slots.

Note that the overall computational requirements associated with this procedure can be considerable, since in practice the matrix equation (8.14) must be solved at several hundred different values of k_z in order to produce the required data prior to inverse Fourier transformation!

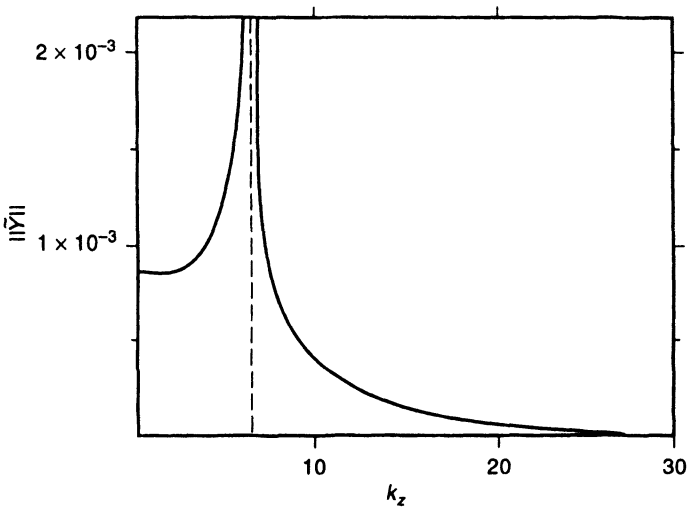

Figure 8.5 Norm of the spectral admittance function for a problem involving circumferential slots of height $0.2\lambda_0$ in a cylinder with $1.0\lambda_0$ radius. After [1]. ©1989 IEEE.

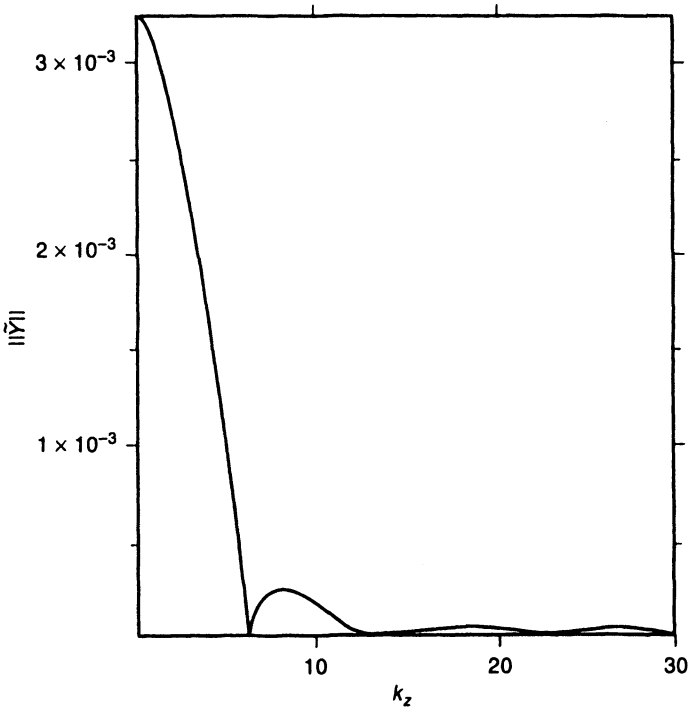

Figure 8.6 Norm of the spectral admittance function for a problem involving axial slots of width $0.686\lambda_0$ in a cylinder with $0.758\lambda_0$ radius.

8.5 OBLIQUE SCATTERING FROM INHOMOGENEOUS CYLINDERS: VOLUME INTEGRAL EQUATION FORMULATION [5]

The previous sections considered the scattering of oblique waves from perfectly conducting cylinders. In this section, we consider a volume integral equation in order to model heterogeneous material. If the cylinder is perfectly conducting, there is no coupling between the TM and TE cases. However, if the cylinder is inhomogeneous, an oblique TE or TM excitation will be depolarized into a combination of both types. Consequently, we combine the TM and TE polarizations in the following approach.

Consider an infinite, z-invariant cylinder characterized by complex-valued relative permittivity and permeability functions $\varepsilon_r(x, y)$ and $\mu_r(x, y)$. The cylinder is illuminated by a source that, in the absence of the cylinder, produces fields with z-components:

$$\hat{z} \cdot \bar{E}^{\text{inc}}(x, y, z) = E_z^{\text{inc}}(x, y)e^{jk_z z} \tag{8.32}$$

$$\hat{z} \cdot \bar{H}^{\text{inc}}(x, y, z) = H_z^{\text{inc}}(x, y)e^{jk_z z} \tag{8.33}$$

Suppose that the cylinder cross section is modeled by triangular cells of constant permittivity and permeability. The dielectric and magnetic material may be replaced by equivalent volumetric polarization currents defined in each cell according to

$$J_z = j\omega\varepsilon_0(\varepsilon_r - 1)E_z \tag{8.34}$$

$$K_z = j\omega\mu_0(\mu_r - 1)H_z \tag{8.35}$$

$$\bar{J}_t = \frac{\varepsilon_r - 1}{k^2\varepsilon_r\mu_r - k_z^2}(-k_z\omega\varepsilon_0\nabla_t E_z - k^2\mu_r\hat{z} \times \nabla_t H_z) \tag{8.36}$$

$$\bar{K}_t = \frac{\mu_r - 1}{k^2\varepsilon_r\mu_r - k_z^2}(k^2\varepsilon_r\hat{z} \times \nabla_t E_z - k_z\omega\mu_0\nabla_t H_z) \tag{8.37}$$

where ∇_t is the transverse gradient $\hat{x}\,\partial/\partial x + \hat{y}\,\partial/\partial y$ and $E_z(x, y)$ and $H_z(x, y)$ are unknown functions that provide the transverse dependence of the total field. Note that all components of the equivalent polarization current density are obtained in terms of just the z-components of the unknown fields, and therefore these z-components are the primary unknowns to be determined.

The equivalent currents of Equations (8.34)–(8.37) radiate in free space but are unknown quantities since they depend on the total field components E_z and H_z. These unknown quantities must satisfy the coupled scalar integral equations

$$E_z^{\text{inc}}(x, y) = E_z(x, y) - \frac{k^2 - k_z^2}{j\omega\varepsilon_0}(J_z * G) - \frac{k_z}{\omega\varepsilon_0}(\nabla_t \cdot \bar{J}_t * G) + (\hat{z} \cdot \nabla_t \times \bar{K}_t * G) \tag{8.38}$$

$$H_z^{\text{inc}}(x, y) = H_z(x, y) - \frac{k^2 - k_z^2}{j\omega\mu_0}(K_z * G) - \frac{k_z}{\omega\mu_0}(\nabla_t \cdot \bar{K}_t * G) - (\hat{z} \cdot \nabla_t \times \bar{J}_t * G) \tag{8.39}$$

where the asterisk denotes two-dimensional convolution, that is,

$$a * b = \int_{-\infty}^{\infty}\int_{-\infty}^{\infty} a(x', y')b(x - x', y - y')\,dx'\,dy' \tag{8.40}$$

and the Green's function is given by

$$G(x, y) = \frac{1}{4j} H_0^{(2)}\left(\sqrt{k^2 - k_z^2}\sqrt{x^2 + y^2}\right) \tag{8.41}$$

where $H_0^{(2)}$ is the zero-order Hankel function of the second kind. Equations (8.38) and (8.39) can be obtained from (1.99) and (1.100) by exchanging all z-derivatives for multiplications with jk_z.

For an arbitrary scatterer, (8.38) and (8.39) can be discretized in the context of the method of moments. We consider an approach similar to that presented in Section 2.7 and employ a piecewise-linear representation of E_z and H_z throughout triangular cells. From a global perspective, linear interpolation between the corners of a triangular cell is equivalent to the expansion of E_z and H_z in the linear pyramid basis functions depicted in Figure 2.20. If $B_n(x, y)$ denotes a pyramid basis function centered at the nth corner or node within the triangular-cell model of the cylinder cross section, the total fields can be expressed as

$$E_z(x, y) \cong \sum_{n=1}^{N} e_n B_n(x, y) \tag{8.42}$$

$$H_z(x, y) \cong \sum_{n=1}^{N} h_n B_n(x, y) \tag{8.43}$$

Since the z-components of the scattered E_z- and H_z-fields will be continuous across cell boundaries, the integral equations can be enforced by point matching at the corners of each cell. This procedure produces a matrix equation of the form

$$\begin{bmatrix} \mathbf{EE} & \mathbf{EH} \\ \mathbf{HE} & \mathbf{HH} \end{bmatrix} \begin{bmatrix} e_1 \\ \vdots \\ e_N \\ h_1 \\ \vdots \\ h_N \end{bmatrix} = \begin{bmatrix} E_z^{\text{inc}}(x_1, y_1) \\ \vdots \\ E_z^{\text{inc}}(x_N, y_N) \\ H_z^{\text{inc}}(x_1, y_1) \\ \vdots \\ H_z^{\text{inc}}(x_N, y_N) \end{bmatrix} \tag{8.44}$$

having entries

$$\begin{aligned} EE_{mn} = {} & \delta_n^m - (k^2 - k_z^2)[(\varepsilon_r - 1)B_n * G]_{x=x_m, y=y_m} \\ & + k_z^2 \left[\nabla_t \cdot \left(\frac{\varepsilon_r - 1}{k^2 \varepsilon_r \mu_r - k_z^2} \nabla_t B_n\right) * G\right]_{x=x_m, y=y_m} \\ & + k^2 \left[\hat{z} \cdot \nabla_t \times \left(\frac{\varepsilon_r(\mu_r - 1)}{k^2 \varepsilon_r \mu_r - k_z^2} \hat{z} \times \nabla_t B_n\right) * G\right]_{x=x_m, y=y_m} \end{aligned} \tag{8.45}$$

$$\begin{aligned} EH_{mn} = {} & \frac{k^2 k_z}{\omega \varepsilon_0} \left[\nabla_t \cdot \left(\frac{(\varepsilon_r - 1)\mu_r}{k^2 \varepsilon_r \mu_r - k_z^2} \hat{z} \times \nabla_t B_n\right) * G\right]_{x=x_m, y=y_m} \\ & - k_z \omega \mu_0 \left[\hat{z} \cdot \nabla_t \times \left(\frac{\mu_r - 1}{k^2 \varepsilon_r \mu_r - k_z^2} \nabla_t B_n\right) * G\right]_{x=x_m, y=y_m} \end{aligned} \tag{8.46}$$

$$HE_{mn} = -\frac{k^2 k_z}{\omega\mu_0}\left[\nabla_t \cdot \left(\frac{(\mu_r - 1)\varepsilon_r}{k^2\varepsilon_r\mu_r - k_z^2}\hat{z} \times \nabla_t B_n\right) * G\right]_{x=x_m, y=y_m} + k_z\omega\varepsilon_0\left[\hat{z} \cdot \nabla_t \times \left(\frac{\varepsilon_r - 1}{k^2\varepsilon_r\mu_r - k_z^2}\nabla_t B_n\right) * G\right]_{x=x_m, y=y_m} \tag{8.47}$$

and

$$HH_{mn} = \delta_n^m - (k^2 - k_z^2)[(\mu_r - 1)B_n * G]_{x=x_m, y=y_m} + k_z^2\left[\nabla_t \cdot \left(\frac{\mu_r - 1}{k^2\varepsilon_r\mu_r - k_z^2}\nabla_t B_n\right) * G\right]_{x=x_m, y=y_m} + k^2\left[\hat{z} \cdot \nabla_t \times \left(\frac{\mu_r(\varepsilon_r - 1)}{k^2\varepsilon_r\mu_r - k_z^2}\hat{z} \times \nabla_t B_n\right) * G\right]_{x=x_m, y=y_m} \tag{8.48}$$

where δ_n^m is the Kronecker delta function. Because the z-components of the fields are linear functions within this representation, transverse fields and transverse current densities are constant within a cell. Furthermore, derivatives of the piecewise-constant functions must be interpreted as generalized functions. As a result, the differential operators in (8.45)–(8.48) produce Dirac delta functions having support limited to the edges between cells. Both convolutions appearing in Equations (8.46) and (8.47) and the last two convolutions in Equations (8.45) and (8.48) involve functions with support only over cell edges. Thus, these are actually one-dimensional convolution integrals. The first convolution in Equation (8.45) and the first convolution in (8.48) are two-dimensional integrals. In general, all of the convolution integrals must be evaluated by numerical quadrature.

Each entry in (8.45)–(8.48) represents a contribution from a source that is distributed over several adjacent cells. The direct evaluation of these expressions, although straightforward, involves redundant computations since the same integrals arise again and again. As previously illustrated in Chapters 2 and 3, it is usually more efficient to adopt an indirect approach in which the necessary integrals are evaluated only once over each cell face or cell edge and then added to the appropriate locations throughout the matrix. The indirect approach is conceptually more difficult to follow, but it requires the minimum data structure to link cells, edges, and corner nodes within a general triangular-cell model.

The coupled integral equation formulation is directly applicable to arbitrary inhomogeneous cylinders, and a variety of results illustrating the accuracy of the formulation have been presented in the literature [5]. The bistatic scattering cross section, defined as

$$\sigma(\phi) = \lim_{\rho\to\infty} 2\pi\rho\frac{|E_z^s(\rho,\phi)|^2 + \eta^2|H_z^s(\rho,\phi)|^2}{|E_z^{\text{inc}}(0,0)|^2 + \eta^2|H_z^{\text{inc}}(0,0)|^2} \tag{8.49}$$

can be computed as a secondary calculation. As an example, consider the oblique scattering from a finite rectangular slab of dimension 2.0λ by 0.1λ, a geometry for which there is no known exact solution. Results for the bistatic scattering cross section are presented in Figure 8.7 for TM incidence and Figure 8.8 for TE incidence for two permittivity profiles, the homogeneous case with $\varepsilon_r = 3 - j0.3$ and $\mu_r = 2 - j0.1$ and an inhomogeneous slab with permittivity and permeability profiles given by

$$\varepsilon_r = 3 - j0.3 + 2\cos(0.5\pi y) \tag{8.50}$$

$$\mu_r = 1 + (1 - j0.05)|y| \tag{8.51}$$

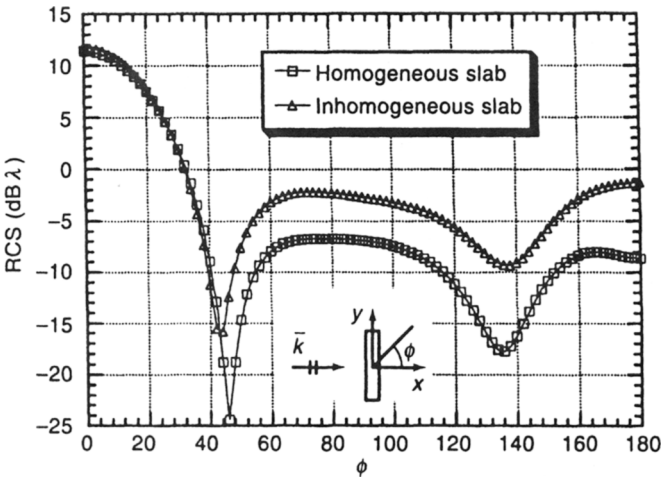

Figure 8.7 Bistatic scattering cross section for an inhomogeneous dielectric cylinder and a homogeneous cylinder when illuminated by a TM wave incident at an oblique angle of 45°. The cylinders are of cross-sectional dimension $2\lambda_0$ by $0.1\lambda_0$. After [5]. ©1991 IEEE.

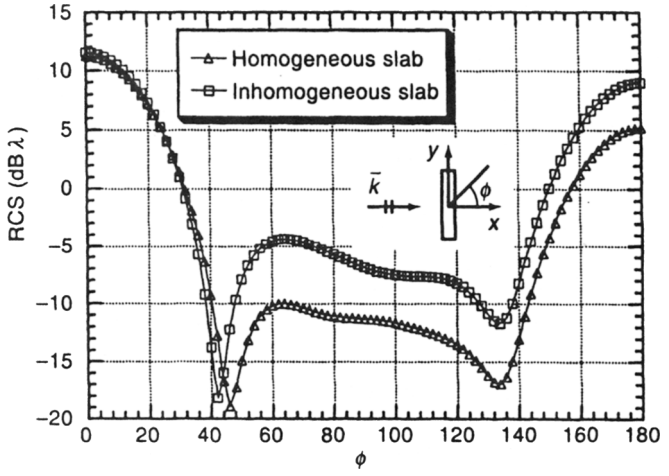

Figure 8.8 Bistatic scattering cross section for the cylinders of Figure 8.7 when illuminated by a TE wave incident at an oblique angle of 45°. After [5]. ©1991 IEEE.

where y is specified in units of wavelength (λ). The y-axis is located along the long dimension of the slab cross section with the origin in the center of the slab. The incident field propagates in the x–z plane (broadside incidence). A triangular-cell model having 50 nodes along the long dimension and 3 nodes across the short dimension is employed, to yield 300 unknowns and a density (for the homogeneous-slab problem) of approximately 250 unknowns per square dielectric wavelength. These curves are in agreement with data from Figure 6 of reference [6].

The preceding formulation may be extended to include closed, perfectly conducting regions imbedded within the cylinder geometry. Perfectly conducting material may be

modeled by an equivalent electric surface current density radiating in the presence of the equivalent polarization currents defined in (8.34)–(8.37). For oblique incidence, both $\hat{z}$- and $\hat{t}$-components of current are excited. Equations (8.38) and (8.39) can be modified to include appropriate surface integrals over the additional sources, and we leave this modification as an exercise for the reader.

If a perfectly conducting region is in direct contact with the dielectric or magnetic material, the H_z-field component at the surface directly defines the transverse electric current density. The linear pyramid function representation for H_z translates into a piecewise-linear representation along the surface, and it is not necessary to introduce additional unknowns to represent transverse currents on the conductor. Although the z-component of the electric current density could in principle be defined by the normal derivative of E_z at the surface of the conductor, approximations inherent in this type of numerical derivative have been found to introduce appreciable error. Thus, an independent expansion can be introduced for the z-component of the surface current in terms of pulse (piecewise-constant) or triangle (piecewise-linear) basis functions defined along each edge of the triangular-cell model bordering the conductor. The coefficients of these basis functions are additional unknowns to be determined. However, E_z should vanish at the surface of a perfect electric conductor, meaning that the coefficients of the pyramid basis functions for E_z along the conductor surface may be set equal to zero. Consequently, the additional unknowns for J_z are balanced by an equal reduction in the number of unknown coefficients for E_z. In summary, the total number of unknowns is given by twice the number of nodes in the triangular-cell model, despite any imbedded conductors.

8.6 OBLIQUE SCATTERING FROM INHOMOGENEOUS CYLINDERS: SCALAR DIFFERENTIAL EQUATION FORMULATION [7]

Volume integral equation formulations, such as the approach of the preceding section, involve fully populated matrix equations and require a relatively large computational effort to treat scatterers of moderate electrical size. Our previous investigation in Chapter 3 suggests that the computational effort associated with differential equation formulations can be significantly less than that required for volume integral formulations, because of the sparse nature of the matrices, and motivates an extension of the scalar differential equation methods to treat oblique scattering.

Figure 8.9 depicts the cross section of an infinite, z-invariant cylinder characterized by complex-valued relative permittivity and permeability functions $\varepsilon_r(x, y)$ and $\mu_r(x, y)$. A conducting region having boundary $\partial\Gamma_c$ is also imbedded within the cylinder. The cylinder is illuminated by an incident electromagnetic field with z-components described by the general form in Equations (8.32) and (8.33). In common with the volume integral formulation of Section 8.5, we suppose that the cylinder cross section is modeled by triangular cells of constant permittivity and permeability. Furthermore, we wish to employ the total fields E_z and H_z as the primary unknowns to be determined and obtain the transverse field components within a homogeneous cell via the relations

$$\bar{E}_t = \frac{1}{k^2\varepsilon_r\mu_r - k_z^2}(j\omega\mu_0\mu_r\hat{z} \times \nabla_t H_z + jk_z\nabla_t E_z) \tag{8.52}$$

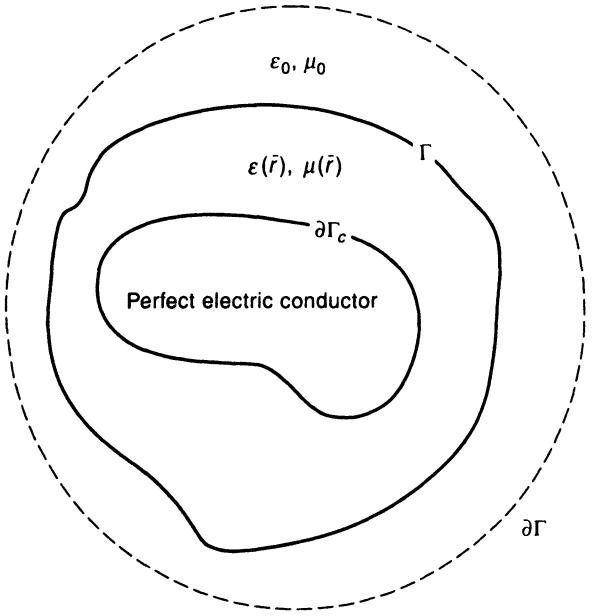

Figure 8.9 Cross section of a general inhomogeneous cylinder.

and

$$\bar{H}_t = \frac{1}{k^2\varepsilon_r\mu_r - k_z^2}(jk_z\nabla_t H_z - j\omega\varepsilon_0\varepsilon_r\hat{z} \times \nabla_t E_z) \tag{8.53}$$

where ∇_t is the transverse gradient.

To derive weak differential equations for E_z and H_z, observe that the fields in the vicinity of the scatterer must satisfy Maxwell's curl equations:

$$\nabla \times \bar{H} = j\omega\varepsilon_0\varepsilon_r\bar{E} \tag{8.54}$$

$$\nabla \times \bar{E} = -j\omega\mu_0\mu_r\bar{H} \tag{8.55}$$

The scalar product of (8.54) and (8.55) with the testing function

$$\bar{T}(x, y, z) = \hat{z}T(x, y) \tag{8.56}$$

can be integrated over the domain Γ to produce

$$\iint_\Gamma \bar{T} \cdot \nabla \times \bar{H} - j\omega\varepsilon_0\varepsilon_r\bar{T} \cdot \bar{E} = 0 \tag{8.57}$$

$$\iint_\Gamma \bar{T} \cdot \nabla \times \bar{E} + j\omega\mu_0\mu_r\bar{T} \cdot \bar{H} = 0 \tag{8.58}$$

The two-dimensional divergence theorem

$$\iint_\Gamma \nabla \cdot (\bar{T} \times \bar{H}) = \int_{\partial\Gamma+\partial\Gamma_c} (\bar{T} \times \bar{H}) \cdot \hat{n} \tag{8.59}$$

and the vector identities

$$\bar{T} \cdot \nabla \times \bar{H} = \nabla \times \bar{T} \cdot \bar{H} - \nabla \cdot (\bar{T} \times \bar{H}) \tag{8.60}$$

and

$$(\bar{T} \times \bar{H}) \cdot \hat{n} = -\bar{T} \cdot (\hat{n} \times \bar{H}) \tag{8.61}$$

can be employed to convert Equations (8.57) and (8.58) into

$$\iint_{\Gamma} \nabla \times \bar{T} \cdot \bar{H}_t - j\omega\varepsilon_0\varepsilon_r TE_z = -\int_{\partial\Gamma+\partial\Gamma_c} \bar{T} \cdot (\hat{n} \times \bar{H}) \tag{8.62}$$

$$\iint_{\Gamma} \nabla \times \bar{T} \cdot \bar{E}_t + j\omega\mu_0\mu_r TH_z = -\int_{\partial\Gamma+\partial\Gamma_c} \bar{T} \cdot (\hat{n} \times \bar{E}) \tag{8.63}$$

where $\partial\Gamma + \partial\Gamma_c$ denotes the entire boundary of the region Γ, with normal $\hat{n}$ pointing out of the region (in accordance with Figure 8.9, $\partial\Gamma_c$ denotes the surface of the imbedded conductor; $\partial\Gamma$ denotes the exterior boundary on which the computational domain is to be truncated). It is assumed that all inhomogeneities are completely enclosed by the exterior boundary.

Following an approach similar to that introduced in Section 3.2, boundary conditions on the imbedded perfect conductor will be incorporated via the surface integrals over $\partial\Gamma_c$. Since the tangential electric field must vanish on the perfectly conducting surface, E_z is a known function on $\partial\Gamma_c$ and satisfies a homogeneous Dirichlet boundary condition. Consequently, all the testing functions used to discretize (8.62) will vanish on $\partial\Gamma_c$, and the boundary integral will contribute nothing to the matrix equation. In the case of the similar boundary integral appearing in Equation (8.63), it is also desired that the tangential electric field vanish on $\partial\Gamma_c$. This is equivalent to a homogeneous Neumann boundary condition and is usually enforced by ignoring the integral over $\partial\Gamma_c$. As a result, the integrals over $\partial\Gamma_c$ in (8.62) and (8.63) will be ignored throughout the rest of the development. Note that an impedance boundary condition can be incorporated on $\partial\Gamma_c$ in an obvious way, in which case the integrals would not vanish. Along a perfectly conducting boundary $\partial\Gamma_c$, the basis function representation for E_z must explicitly satisfy the zero boundary condition. In contrast, no special conditions are to be imposed on the expansion for H_z along $\partial\Gamma_c$. While E_z is known along the conducting boundary, H_z is an unknown function on the surface.

The expressions for transverse fields in Equations (8.52) and (8.53) may be substituted into (8.62) and (8.63) and combined with the vector identity

$$\nabla \times \bar{T} = -\hat{z} \times \nabla_t T \tag{8.64}$$

to cast the resulting equations into the form

$$\iint_{\Gamma} \frac{\varepsilon_r}{\varepsilon_r\mu_r - (k_z^2/k^2)} \nabla_t T \cdot \nabla_t E_z - k^2\varepsilon_r TE_z + \iint_{\Gamma} \frac{-k_z}{\omega\varepsilon_0} \frac{1}{\varepsilon_r\mu_r - (k_z^2/k^2)} \hat{z} \cdot \nabla_t T \times \nabla_t H_z = -\int_{\partial\Gamma} \bar{T} \cdot \hat{n} \times \nabla \times \bar{E} \tag{8.65}$$

and

$$\iint_{\Gamma} \frac{\mu_r}{\varepsilon_r\mu_r - (k_z^2/k^2)} \nabla_t T \cdot \nabla_t H_z - k^2\mu_r TH_z + \iint_{\Gamma} \frac{k_z}{\omega\mu_0} \frac{1}{\varepsilon_r\mu_r - (k_z^2/k^2)} \hat{z} \cdot \nabla_t T \times \nabla_t E_z = -\int_{\partial\Gamma} \bar{T} \cdot \hat{n} \times \nabla \times \bar{H} \tag{8.66}$$

Equations (8.65) and (8.66) constitute coupled weak differential equations describing the electromagnetic fields throughout the region Γ in terms of the total fields on the boundary $\partial\Gamma$. For a normally incident excitation, these equations reduce to (3.5) for the TM polarization and (3.6) for the TE polarization. In order to represent the complete scattering problem, it is necessary to augment these equations with additional information about the fields on $\partial\Gamma$. For instance, an inward-looking formulation can be obtained by combining these equations with an appropriate surface integral equation or eigenfunction expansion representing the

exterior region, as described in Section 3.12. On the other hand, an outward-looking formulation can be obtained by incorporating some type of RBC directly into the boundary integrals.

We limit our investigation to one specific outward-looking approach and for simplicity assume that the boundary $\partial\Gamma$ is circular with radius a. An exact RBC can be derived from an exterior eigenfunction expansion following the procedure of Section 3.3, and we leave the details of the development to the reader (Prob. P8.9). For the case of oblique excitation, the pertinent RBCs can be written as

$$\begin{aligned}\hat{z}\cdot\hat{\rho}\times(\nabla\times\bar{E})|_{(a,\phi,0)} = {} & \frac{1}{2\pi}\int_0^{2\pi} E_z(a,\phi')K_1(\phi-\phi')\,d\phi' \\ & + \eta\frac{1}{2\pi}\int_0^{2\pi} H_z(a,\phi')K_2(\phi-\phi')\,d\phi' \\ & + \frac{1}{2\pi}\int_0^{2\pi} E_z^{\text{inc}}(a,\phi')K_3(\phi-\phi')\,d\phi'\end{aligned} \tag{8.67}$$

and

$$\begin{aligned}\hat{z}\cdot\hat{\rho}\times(\nabla\times\bar{H})|_{(a,\phi,0)} = {} & \frac{1}{2\pi}\int_0^{2\pi} H_z(a,\phi')K_1(\phi-\phi')\,d\phi' \\ & - \frac{1}{\eta}\frac{1}{2\pi}\int_0^{2\pi} E_z(a,\phi')K_2(\phi-\phi')\,d\phi' \\ & + \frac{1}{2\pi}\int_0^{2\pi} H_z^{\text{inc}}(a,\phi')K_3(\phi-\phi')\,d\phi'\end{aligned} \tag{8.68}$$

where the kernels are defined as

$$K_1(\phi) = -\frac{k^2}{k_t}\sum_{n=-\infty}^{\infty}\frac{H_n^{(2)\prime}(k_t a)}{H_n^{(2)}(k_t a)}e^{jn\phi} \tag{8.69}$$

$$K_2(\phi) = \frac{jkk_z}{k_t^2 a}\sum_{n=-\infty}^{\infty} ne^{jn\phi} \tag{8.70}$$

$$K_3(\phi) = -\frac{j2k^2}{\pi k_t^2 a}\sum_{n=-\infty}^{\infty}\frac{1}{J_n(k_t a)H_n^{(2)}(k_t a)}e^{jn\phi} \tag{8.71}$$

and where

$$k_t = \sqrt{k^2 - k_z^2} \tag{8.72}$$

Although the summations appearing in Equations (8.69) and (8.70) are divergent, the required calculations in Equations (8.67) and (8.68) involve only integrals over these kernels. Because the fields are well behaved on $\partial\Gamma$, the cylindrical harmonic content of the functions $E_z(\phi)$ and $H_z(\phi)$ ensures that the integrals are convergent and relatively easy to compute.

Equations (8.67) and (8.68) may be substituted into the boundary integrals in (8.65) and (8.66) to complete the formulation. The resulting equations can be discretized following the finite-element procedure using a piecewise-linear representation for E_z and H_z and

piecewise-linear testing functions, to produce the matrix equation

$$\begin{bmatrix} \mathbf{A} & \mathbf{B} \\ \mathbf{C} & \mathbf{D} \end{bmatrix} \begin{bmatrix} e \\ h \end{bmatrix} = \begin{bmatrix} e^{\text{inc}} \\ h^{\text{inc}} \end{bmatrix} \tag{8.73}$$

where

$$A_{mn} = \iint_{\Gamma} \frac{\varepsilon_r}{\varepsilon_r \mu_r - (k_z^2/k^2)} \nabla_t B_m \cdot \nabla_t B_n - k^2 \varepsilon_r B_m B_n - \frac{k^2 a}{2\pi k_t} \sum_{q=-\infty}^{\infty} \frac{H_q^{(2)\prime}(k_t a)}{H_q^{(2)}(k_t a)} I_m(q) I_n(-q) \tag{8.74}$$

$$B_{mn} = \iint_{\Gamma} \frac{-k_z}{\omega \varepsilon_0} \frac{1}{\varepsilon_r \mu_r - (k_z^2/k^2)} \hat{z} \cdot \nabla_t B_m \times \nabla_t B_n + \frac{jkk_z\eta}{2\pi k_t^2} \sum_{q=-\infty}^{\infty} q I_m(q) I_n(-q) \tag{8.75}$$

$$C_{mn} = \iint_{\Gamma} \frac{k_z}{\omega \mu_0} \frac{1}{\varepsilon_r \mu_r - (k_z^2/k^2)} \hat{z} \cdot \nabla_t B_m \times \nabla_t B_n - \frac{jkk_z}{2\pi k_t^2 \eta} \sum_{q=-\infty}^{\infty} q I_m(q) I_n(-q) \tag{8.76}$$

and

$$D_{mn} = \iint_{\Gamma} \frac{\mu_r}{\varepsilon_r \mu_r - (k_z^2/k^2)} \nabla_t B_m \cdot \nabla_t B_n - k^2 \mu_r B_m B_n - \frac{k^2 a}{2\pi k_t} \sum_{q=-\infty}^{\infty} \frac{H_q^{(2)\prime}(k_t a)}{H_q^{(2)}(k_t a)} I_m(q) I_n(-q) \tag{8.77}$$

where

$$I_m(q) = \int_{\partial\Gamma} B_m(\phi) e^{jq\phi}\, d\phi \tag{8.78}$$

only contributes to the preceding expressions if node m is located on the boundary $\partial\Gamma$.

Assuming the excitation is a uniform plane wave of the form

$$\begin{Bmatrix} E_z^{\text{inc}} \\ H_z^{\text{inc}} \end{Bmatrix} = \begin{Bmatrix} e_0 \\ h_0 \end{Bmatrix} e^{-jk_t(x\cos\theta + y\sin\theta)} e^{jk_z z} = \begin{Bmatrix} e_0 \\ h_0 \end{Bmatrix} \sum_{q=-\infty}^{\infty} j^{-q} J_q(k_t a) e^{jq\phi} e^{-jq\theta} e^{jk_z z} \tag{8.79}$$

the entries of the excitation vector are given by

$$e_m^{\text{inc}} = \frac{j2k^2 e_0}{\pi k_t^2} \sum_{q=-\infty}^{\infty} \frac{j^{-q} e^{-jq\theta}}{H_q^{(2)}(k_t a)} I_m(q) \tag{8.80}$$

and

$$h_m^{\text{inc}} = \frac{j2k^2 h_0}{\pi k_t^2} \sum_{q=-\infty}^{\infty} \frac{j^{-q} e^{-jq\theta}}{H_q^{(2)}(k_t a)} I_m(q) \tag{8.81}$$

The element matrix entries required for the finite-element system have been previously discussed in Chapter 3, with the sole exception of the integral

$$E_{mn} = \iint_{\Gamma} \hat{z} \cdot \nabla_t T_m \times \nabla_t B_n \, dx \, dy \tag{8.82}$$

Equation (8.82) can be evaluated over a triangular cell using the simplex coordinates (L_1, L_2, L_3) defined in Equations (3.48)–(3.51) of Section 3.7. Using Equation (3.57), we immediately obtain

$$E_{mn} = \frac{b_m c_n - c_m b_n}{4A} \tag{8.83}$$

where A denotes the area of the cell and $\{b_n\}$ and $\{c_n\}$ are functions of the cell shape defined in (3.50) and (3.51).

We will illustrate the performance of this outward-looking formulation by comparing some numerical results with those obtained using the volume integral approach from Section 8.5. Table 8.3 shows numerical values of the E_z-field within a circular, homogeneous dielectric cylinder having $k_t a = 1$ and relative permittivity $\varepsilon_r = 4 - j1$. Results obtained from the volume integral formulation of Section 8.5 and the volume differential formulation of this section using an identical model for the cylinder cross section are compared with the exact solution. The 121-node, 204-cell model contains approximately 369 nodes/λ_d^2. The excitation is purely TM and is incident at an oblique angle of 45° with respect to the cylinder axis. The two numerical results exhibit excellent agreement with each other and the exact solution and demonstrate once again that the accuracy of differential and integral equation formulations is comparable for a similar basis function set.

TABLE 8.3 E_z-Field Produced by Incident TM Plane Wave Along $y = 0$ Cut Through Center of Circular, Homogeneous Dielectric Cylinder Having $k_t a = 1$ and Relative Permittivity $\varepsilon_r = 4 - j1$.

x	Magnitude of E_z			Phase of E_z		
	Integral	Differential	Exact	Integral	Differential	Exact
−0.159	0.934	0.937	0.931	30.74	30.49	30.61
−0.128	0.925	0.927	0.923	11.83	11.61	11.72
−0.096	0.903	0.905	0.902	−8.09	−8.25	−8.22
−0.064	0.891	0.892	0.889	−29.49	−29.59	−29.63
−0.032	0.911	0.912	0.908	−51.59	−51.63	−51.75
0.0	0.974	0.974	0.969	−72.38	−72.41	−72.64
0.032	1.066	1.066	1.060	−90.24	−90.27	−90.61
0.064	1.159	1.158	1.152	−104.80	−104.83	−105.27
0.096	1.222	1.222	1.215	−116.58	−116.61	−117.12
0.128	1.234	1.234	1.227	−126.32	−126.35	−126.91
0.159	1.179	1.182	1.174	−134.62	−134.72	−135.23

Note: Results obtained from the volume integral formulation of Section 8.5 and the volume differential formulation of this section using the identical 161-node model are compared with the exact solution. The excitation is incident at an oblique angle of 45° with respect to the cylinder axis.

As a second example, consider a high-contrast circular cylinder with $k_t a = 0.25$ and relative permittivity $\varepsilon_r = 50 - j20$ (a possible model for muscle tissue at microwave

frequencies). Numerical results for this geometry also exhibit excellent agreement with the integral equation formulation of Section 8.5 and with the exact eigenfunction solution. For illustration, Figure 8.10 shows a plot of the E_z-field produced along the outer surface of the cylinder in response to a TE wave incident at an oblique angle of 30°. These data were obtained using a cylinder model containing 138 triangular cells and a density of 317 nodes/λ_d^2. Even for the large-magnitude relative permittivity employed in this example, both numerical results exhibit excellent agreement with the exact eigenfunction series solution. In addition, the nonzero E_z-component clearly shows the depolarization occurring for oblique scattering, since the excitation in this case is purely TE.

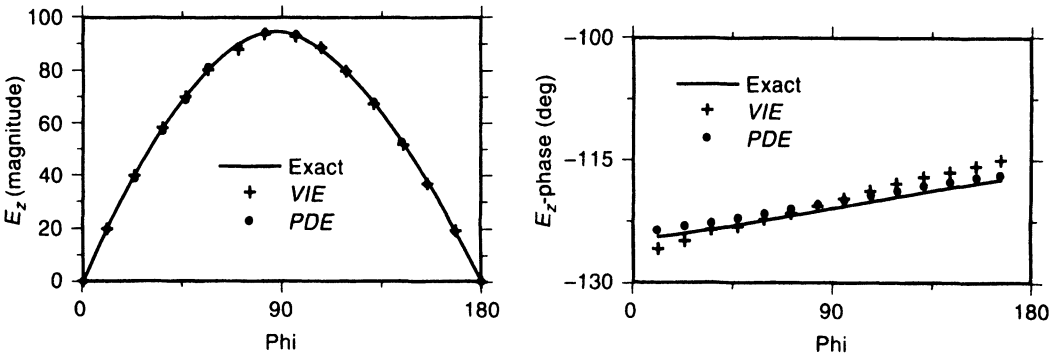

Figure 8.10 The E_z-field produced on the surface of a circular dielectric cylinder with $ka = 0.25$ and $\varepsilon_r = 50 - j20$ by a TE wave incident at an oblique angle of 30°. After [8]. ©1994 IEEE.

8.7 SCATTERING FROM A FINITE-LENGTH, HOLLOW CONDUCTING RIGHT-CIRCULAR CYLINDER: THE BODY-OF-REVOLUTION EFIE FORMULATION [9]

Preceding examples have considered infinite cylinders illuminated by a source that is a function of z. Although the resulting problem is three dimensional in nature, a Fourier decomposition along the cylinder axis can be used to reduce the problem to a superposition of two-dimensional problems more amenable to numerical solution. Axisymmetric scatterers illuminated by a general incident field can also be treated by the superposition of two-dimensional problems. Since the surface of an axisymmetric geometry can be obtained by rotating a "generating arc" around an axis, these structures are often described as *bodies of revolution.*[1] Assuming that the axis of revolution coincides with the z-axis in a cylindrical system, a Fourier series in ϕ can be employed to recast the problem into one involving uncoupled equations for each harmonic.

The body-of-revolution formulation will be illustrated by one simple geometry: a finite-length, hollow, perfectly conducting circular cylinder. The perfectly conducting material may be modeled by equivalent electric currents radiating in free space. Using the coordinate system defined in Figure 8.11, the current density contains both $\hat{z}$- and $\hat{\phi}$-components. Figure 8.11 also depicts the discretization of the cylinder surface as a function

[1]The term "body of revolution" is not intended to imply physical motion of the scatterer.

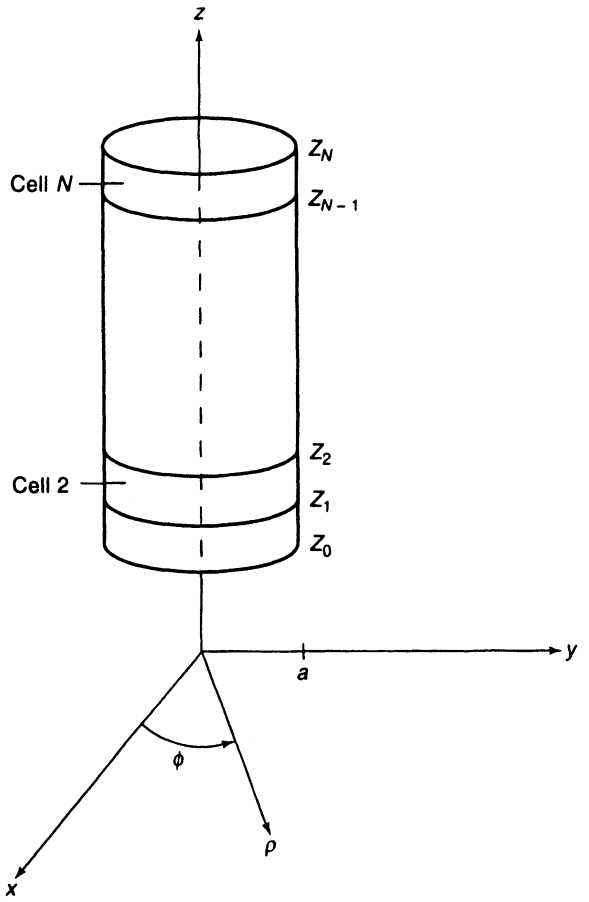

Figure 8.11 Geometry of the hollow cylinder under consideration.

of z. A suitable form of the EFIE is given by

$$\hat{n} \times \bar{E}^{\text{inc}} = -\hat{n} \times (-j\omega\mu_0 \bar{A} - \nabla\Phi_e) \tag{8.84}$$

where $\hat{n}$ is the outward normal vector at the cylinder surface. The magnetic vector and electric scalar potentials are defined as

$$\bar{A}(a, \phi, z) = \int_{z'=z_0}^{z_N} \int_{\phi'=0}^{2\pi} \bar{J}(\phi', z') \frac{e^{-jkR}}{4\pi R} a \, d\phi' \, dz' \tag{8.85}$$

and

$$\Phi_e(a, \phi, z) = \frac{-1}{j\omega\varepsilon_0} \int_{z'=z_0}^{z_N} \int_{\phi'=0}^{2\pi} (\nabla' \cdot \bar{J}) \frac{e^{-jkR}}{4\pi R} a \, d\phi' \, dz' \tag{8.86}$$

where

$$R = \sqrt{(z - z')^2 + 4a^2 \sin^2[\tfrac{1}{2}(\phi - \phi')]} \tag{8.87}$$

Note that Equation (8.84) is valid only on the surface of the original cylinder.

Because the unknown current densities, the incident fields, and the Green's function are periodic in ϕ, these quantities can each be expressed as a Fourier series according to

$$J_\phi(\phi', z') = \sum_{m=-\infty}^{\infty} J_{\phi m}(z') e^{jm\phi'} \tag{8.88}$$

$$J_z(\phi', z') = \sum_{m=-\infty}^{\infty} J_{zm}(z') e^{jm\phi'} \tag{8.89}$$

$$E_\phi^{\text{inc}}(\phi, z) = \sum_{m=-\infty}^{\infty} E_{\phi m}^{\text{inc}}(z) e^{jm\phi} \tag{8.90}$$

$$E_z^{\text{inc}}(\phi, z) = \sum_{m=-\infty}^{\infty} E_{zm}^{\text{inc}}(z) e^{jm\phi} \tag{8.91}$$

and

$$\frac{e^{-jkR}}{4\pi R} = \sum_{m=-\infty}^{\infty} G_m(z - z') e^{jm(\phi - \phi')} \tag{8.92}$$

where $J_{\phi m}(z')$ and $J_{zm}(z')$ are unknowns to be determined,

$$E_{\phi m}^{\text{inc}}(z) = \frac{1}{2\pi} \int_{\alpha=-\pi}^{\pi} E_\phi^{\text{inc}}(a, \alpha, z) e^{-jm\alpha}\, d\alpha \tag{8.93}$$

$$E_{zm}^{\text{inc}}(z) = \frac{1}{2\pi} \int_{\alpha=-\pi}^{\pi} E_z^{\text{inc}}(a, \alpha, z) e^{-jm\alpha}\, d\alpha \tag{8.94}$$

and

$$G_m(z - z') = \frac{1}{2\pi} \int_{\alpha=-\pi}^{\pi} \frac{e^{-jk\tilde{R}}}{4\pi \tilde{R}} e^{-jm\alpha}\, d\alpha \tag{8.95}$$

Equation (8.95) can be simplified to

$$G_m(z - z') = \frac{1}{4\pi^2} \int_{\alpha=0}^{\pi} \frac{e^{-jk\tilde{R}}}{\tilde{R}} \cos(m\alpha)\, d\alpha \tag{8.96}$$

where

$$\tilde{R} = \sqrt{(z - z')^2 + 4a^2 \sin^2(\tfrac{1}{2}\alpha)} \tag{8.97}$$

By substituting the above expansions into the integral equation and taking an inner product of both sides with an individual Fourier harmonic such as

$$\frac{1}{2\pi} e^{-jp\phi} \tag{8.98}$$

the original equation is separated into independent equations for each of the Fourier harmonics $J_{\phi m}$ and J_{zm}. The coupled system for the mth harmonic can be written as

$$-E_{\phi m}^{\text{inc}}(z) = \frac{2\pi a}{j\omega\varepsilon_0}\int_{z'=z_0}^{z_N}\left\{k^2 J_{\phi m}(z')\frac{G_{m-1}(z-z')+G_{m+1}(z-z')}{2} + \left[-\frac{m^2}{a^2}J_{\phi m}(z') + j\frac{m}{a}\frac{\partial J_{zm}}{\partial z'}\right]G_m(z-z')\right\}dz' \tag{8.99}$$

$$-E_{zm}^{\text{inc}}(z) = \frac{2\pi a}{j\omega\varepsilon_0}\int_{z'=z_0}^{z_N} k^2 J_{zm}(z')G_m(z-z')\,dz' + \frac{2\pi a}{j\omega\varepsilon_0}\frac{\partial}{\partial z}\int_{z'=z_0}^{z_N}\left[j\frac{m}{a}J_{\phi m}(z') + \frac{\partial J_{zm}}{\partial z'}\right]G_m(z-z')\,dz' \tag{8.100}$$

We will consider a general plane-wave incident field of the form

$$\bar{E}^{\text{inc}} = [u_y\hat{y} + u_\theta(\hat{x}\cos\theta_i + \hat{z}\sin\theta_i)]e^{-jk(z\cos\theta_i - x\sin\theta_i)} \tag{8.101}$$

where θ is the usual spherical angle measured from the z-axis. After substituting (8.101) into Equations (8.93) and (8.94), we obtain

$$E_{zm}^{\text{inc}}(z) = u_\theta \sin\theta_i j^m J_m(ka\sin\theta_i)e^{-jkz\cos\theta_i} \tag{8.102}$$

and

$$E_{\phi m}^{\text{inc}}(z) = \tfrac{1}{2}\{u_\theta\cos\theta_i j^m[J_{m-1}(ka\sin\theta_i) + J_{m+1}(ka\sin\theta_i)] + u_y j^{m-1}[J_{m-1}(ka\sin\theta_i) - J_{m+1}(ka\sin\theta_i)]\}e^{-jkz\cos\theta_i} \tag{8.103}$$

as explicit expressions for the mth harmonics. These expression were obtained using

$$\int_0^\pi e^{jka\cos\phi\sin\theta_i}\cos(m\phi)\,d\phi = j^m\pi J_m(ka\sin\theta_i) \tag{8.104}$$

where J_m is the ordinary Bessel function.

Equations (8.99) and (8.100) must be solved for each of the significant harmonics excited by the incident field, after which the solutions for $J_{\phi m}$ and J_{zm} may be superimposed to produce the total current density.

If the cylinder is divided into cells along the z direction as illustrated in Figure 8.11, the unknown current densities may be expanded in basis functions

$$J_{\phi m}(z) \cong \sum_{n=1}^{N} j_{\phi n}p(z; z_{n-1}, z_n) \tag{8.105}$$

$$J_{zm}(z) \cong \sum_{n=1}^{N-1} j_{zn}t(z; z_{n-1}, z_n, z_{n+1}) \tag{8.106}$$

where $p(z; z_1, z_2)$ and $t(z; z_1, z_2, z_3)$ are subsectional pulse and triangle functions defined in Figure 5.1. If these expansions are substituted into (8.99) and (8.100), the resulting equations may be enforced approximately via an inner product with the testing functions

$$T_\phi^p(z) = (\Delta z)_p\delta[z - \tfrac{1}{2}(z_{p-1} + z_p)] \tag{8.107}$$

$$T_z^p(z) = p(z; \tfrac{1}{2}(z_{p-1} + z_p), \tfrac{1}{2}(z_p + z_{p+1})) \tag{8.108}$$

to produce the $(2N-1)\times(2N-1)$ matrix equation

$$\begin{bmatrix} \mathbf{A} & \mathbf{B} \\ \mathbf{C} & \mathbf{D} \end{bmatrix} \begin{bmatrix} \mathbf{j}_\phi \\ \mathbf{j}_z \end{bmatrix} = \begin{bmatrix} \mathbf{E}_\phi^{\text{inc}} \\ \mathbf{E}_z^{\text{inc}} \end{bmatrix} \tag{8.109}$$

where

$$E_{\phi p}^{\text{inc}} = -(\Delta z)_p E_{\phi m}^{\text{inc}}[\tfrac{1}{2}(z_{p-1}+z_p)] \qquad p = 1, 2, \ldots, N \tag{8.110}$$

$$E_{zp}^{\text{inc}} = -\int_{(z_{p-1}+z_p)/2}^{(z_p+z_{p+1})/2} E_{zm}^{\text{inc}}(z)\, dz \qquad p = 1, 2, \ldots, N-1 \tag{8.111}$$

$$\begin{aligned} A_{pn} = -ja\eta(\Delta z)_p \Bigg\{ & \frac{m^2}{a^2} \int_{z_{n-1}}^{z_n} G_m\left(\frac{z_{p-1}+z_p}{2} - z'\right) dz' \\ & - k^2 \int_{z_{n-1}}^{z_n} \frac{1}{2}\left[G_{m-1}\left(\frac{z_{p-1}+z_p}{2} - z'\right) \right. \\ & \left. + G_{m+1}\left(\frac{z_{p-1}+z_p}{2} - z'\right)\right] dz' \Bigg\} \end{aligned} \tag{8.112}$$

$$n = 1, 2, \ldots, N \qquad p = 1, 2, \ldots, N$$

$$\begin{aligned} B_{pn} = (\Delta z)_p m\eta \Bigg\{ & \frac{1}{(\Delta z)_n} \int_{z_{n-1}}^{z_n} G_m\left(\frac{z_{p-1}+z_p}{2} - z'\right) dz' \\ & - \frac{1}{(\Delta z)_{n+1}} \int_{z_n}^{z_{n+1}} G_m\left(\frac{z_{p-1}+z_p}{2} - z'\right) dz' \Bigg\} \end{aligned} \tag{8.113}$$

$$n = 1, 2, \ldots, N-1 \qquad p = 1, 2, \ldots, N$$

$$C_{pn} = m\eta \left\{ \int_{z_{n-1}}^{z_n} G_m\left(\frac{z_p+z_{p+1}}{2} - z'\right) dz' - \int_{z_{n-1}}^{z_n} G_m\left(\frac{z_{p-1}+z_p}{2} - z'\right) dz' \right\} \tag{8.114}$$

$$n = 1, 2, \ldots, N \qquad p = 1, 2, \ldots, N-1$$

and

$$\begin{aligned} D_{pn} = -ja\eta \Bigg\{ & k^2 \int_{(z_{p-1}+z_p)/2}^{(z_p+z_{p+1})/2} \int_{z_{n-1}}^{z_{n+1}} t(z'; z_{n-1}, z_n, z_{n+1}) G_m(z-z')\, dz'\, dz \\ & + \frac{1}{(\Delta z)_n} \int_{z_{n-1}}^{z_n} G_m\left(\frac{z_p+z_{p+1}}{2} - z'\right) - G_m\left(\frac{z_{p-1}+z_p}{2} - z'\right) dz' \\ & + \frac{1}{(\Delta z)_{n+1}} \int_{z_n}^{z_{n+1}} G_m\left(\frac{z_{p-1}+z_p}{2} - z'\right) - G_m\left(\frac{z_p+z_{p+1}}{2} - z'\right) dz' \Bigg\} \end{aligned} \tag{8.115}$$

$$p = 1, 2, \ldots, N-1 \qquad n = 1, 2, \ldots, N-1$$

where G_m is defined in Equation (8.96).

Because of the regular nature of the scatterer, it is possible to restrict the cells in the model to identical lengths Δz without loss of generality. Under this condition, the above

expressions can be simplified to produce

$$A_{pn} = -ja\eta\left(k^2(\Delta z)K^m_{p-n} - \frac{m^2}{a^2}(\Delta z)I^m_{p-n}\right) \tag{8.116}$$

$$B_{pn} = m\eta(I^m_{p-n} - I^m_{p-n-1}) \tag{8.117}$$

$$C_{pn} = m\eta(I^m_{p-n+1} - I^m_{p-n}) \tag{8.118}$$

$$D_{pn} \cong -ja\eta\left(k^2(\Delta z)I^m_{p-n} + \frac{1}{(\Delta z)}(I^m_{p-n+1} - 2I^m_{p-n} + I^m_{p-n-1})\right) \tag{8.119}$$

where

$$I^m_q = \int_{-\Delta z/2}^{\Delta z/2} G_m(q\ \Delta z - z')\, dz' \tag{8.120}$$

and

$$K^m_q = \tfrac{1}{2}(I^{m-1}_q + I^{m+1}_q) \tag{8.121}$$

Equation (8.119) involves an approximation similar to that used with the EFIE formulation described in Section 2.4. The triple integral appearing in (8.115) has been replaced by a double integral for convenience. Although this approximation is not essential, it permits all the matrix entries to be obtained from a common subroutine implementing Equation (8.120). The error associated with this approximation should decrease as the cell size Δ_z shrinks.

The integrand in (8.120) is singular for the $q = 0$ case and requires special treatment. For $q = 0$, the integral can be expressed as the sum of three parts according to

$$\begin{aligned} I^m_0 = {} & \frac{1}{2\pi^2}\int_0^{\Delta z/2}\int_0^{\pi} \frac{\cos(m\alpha)e^{-jk\tilde{R}} - 1}{\tilde{R}}\, d\alpha\, dz \\ & + \frac{1}{2\pi^2}\int_0^{\Delta z/2}\left[\int_0^{\pi}\frac{1}{\tilde{R}}\, d\alpha + \frac{1}{a}\ln\left(\frac{z}{8a}\right)\right] dz \\ & - \frac{1}{2\pi^2}\int_0^{\Delta z/2}\frac{1}{a}\ln\left(\frac{z}{8a}\right) dz \end{aligned} \tag{8.122}$$

The first integral can be evaluated by numerical quadrature, since for small values of $\tilde{R}$ the integrand becomes

$$-\frac{\tilde{R}}{2}\left(k^2 + \frac{m^2\alpha^2}{z^2 + a^2\alpha^2}\right) - jk\cos(m\alpha) \to -jk\cos(m\alpha) \tag{8.123}$$

which is finite. The second integral can be simplified to

$$\frac{1}{2\pi^2}\int_0^{\Delta z/2}\left[\frac{\sqrt{w}}{a}E(w) + \frac{1}{a}\ln\left(\frac{z}{8a}\right)\right] dz \tag{8.124}$$

where

$$E(w) = \int_0^{\pi/2}\frac{d\beta}{\sqrt{1 - w\sin^2\beta}} \tag{8.125}$$

is the complete elliptic integral of the first kind, and

$$w = \frac{4a^2}{z^2 + 4a^2} \tag{8.126}$$

Here, $E(w)$ can be calculated using a polynomial approximation [10]. It can be shown that the two terms in (8.124) cancel as $z \to 0$, leaving a finite integrand that can be evaluated by quadrature. The final integral in (8.122) is easily evaluated analytically, to yield

$$-\frac{1}{2\pi^2}\int_0^{\Delta z/2}\frac{1}{a}\ln\left(\frac{z}{8a}\right)dz = \frac{\Delta z}{4\pi^2 a}\left[1-\ln\left(\frac{\Delta z}{16a}\right)\right] \tag{8.127}$$

For the case where the integrand is nonsingular, (8.120) may be evaluated using two-dimensional quadrature.

If the cell size Δz is identical throughout the model, the submatrices of the system in (8.109) are highly structured due to the manner in which the integral equation was discretized. In fact, **A** and **D** are symmetric Toeplitz matrices, that is,

$$\mathbf{A} = \begin{bmatrix} a_0 & a_1 & a_2 & \cdots & a_{N-1} \\ a_1 & a_0 & a_1 & \ddots & \cdot \\ a_2 & a_1 & a_0 & & \cdot \\ \vdots & & & & \vdots \\ a_{N-1} & \cdots & \cdots & \cdots & a_0 \end{bmatrix} \tag{8.128}$$

The **B**-matrix can be expressed as

$$\mathbf{B} = \begin{bmatrix} -b_1 & -b_2 & -b_3 & \cdots & -b_{N-1} \\ b_1 & -b_1 & -b_2 & \ddots & \cdot \\ b_2 & b_1 & -b_1 & & \cdot \\ \cdot & & & & \cdot \\ \cdot & & & & -b_1 \\ b_{N-1} & \cdots & \cdots & \cdots & b_1 \end{bmatrix} \tag{8.129}$$

and **C** and **B** are related by

$$\mathbf{C} = -\mathbf{B}^T \tag{8.130}$$

Because of these symmetries, all of the elements of the above matrices can be generated from the first rows of the **A**, **B**, and **D** systems. This amounts to a substantial degree of redundancy that can be exploited to reduce the computation associated with generating the matrix entries. In addition, iterative algorithms such as the CG–FFT procedure (Section 4.12) are easily incorporated into the formulation in order to minimize memory requirements [9].

Equation (8.109) must be solved for all of the significant Fourier harmonics excited by the incident field, including both positive and negative values of m. From an inspection of (8.120), we observe that

$$I_q^m = I_q^{-m} = I_{-q}^m = I_{-q}^{-m} \tag{8.131}$$

and

$$K_q^m = K_q^{-m} = K_{-q}^m = K_{-q}^{-m} \tag{8.132}$$

Thus, the **A** and **D** submatrices are independent of the sign of m, while the **B** and **C** submatrices are proportional to the sign of m. In addition, Bessel functions have the

property

$$J_{-m}(x) = (-1)^m J_m(x) \tag{8.133}$$

which means that

$$E^{\text{inc}}_{z(-m)} = E^{\text{inc}}_{z(m)} \tag{8.134}$$

$$E^{\text{inc}}_{\phi m} = E^m_\theta u_\theta + E^m_y u_y \tag{8.135}$$

and

$$E^{\text{inc}}_{\phi(-m)} = -E^m_\theta u_\theta + E^m_y u_y \tag{8.136}$$

These relations can be used to minimize the required computations.

After the harmonics of the current density are found for all necessary values of m, other parameters such as the scattering cross section can be computed. If the bistatic scattering cross section is to be computed at many observation angles, it is probably desirable to first find the total current density by summing over the harmonics and then compute the scattering cross section according to the formulas of Chapter 1 [Equations (1.157)–(1.159)]. The current must be sampled at a sufficient density of points around the cylinder circumference. As an alternative, the Fourier harmonics of the far-zone fields can be computed directly from the solutions $J_{\phi m}$ and J_{zm} and superimposed to compute the scattering cross section at the observation angles of interest.

As an application of this approach, Figure 8.12 shows the current density induced by an axially incident plane wave on conducting cylinders of radius 0.1λ and 0.6λ. Since the geometry is an infinitesimally thin conducting shell, the EFIE results show the superposition of the current density on the inside and outside of the cylinder. In the first case, the cylinder radius is small enough to suppress any interior circular waveguide modes, and the current exhibits good agreement with the physical optics approximation

$$\bar{J} \cong 2\hat{n} \times \bar{H}^{\text{inc}} \tag{8.137}$$

In the second case, the cylinder radius is larger and an interior mode is excited by the incident field. The waveguide mode propagates with a different effective wavenumber than the exterior field, and the interference between the interior and exterior currents is easily observed in Figure 8.12.

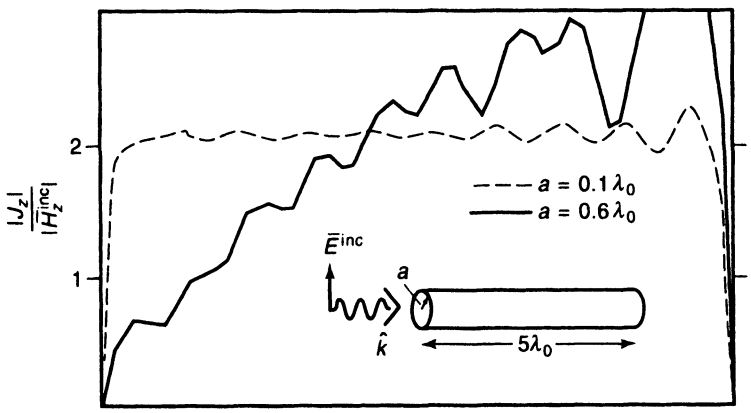

Figure 8.12 Current density (EFIE result) on hollow p.e.c. cylinders.

This example illustrates a surface integral body-of-revolution formulation for a very simple geometry. We will leave the extension to arbitrary axisymmetric scatterers as an exercise for the reader, after noting that general approaches are well established and may be found in the literature [11–14].

8.8 DIFFERENTIAL EQUATION FORMULATION FOR AXISYMMETRIC SCATTERERS [15]

To complement the integral equation formulation of the preceding section, we also present a thumbnail sketch of a differential equation approach for axisymmetric scatterers. For simplicity, we make the additional assumption that the incident field is also axisymmetric, which permits us to employ a pseudoscalar formulation in terms of the ϕ-components of the fields even in the presence of inhomogeneous materials. The approach is general enough to treat problems such as a monopole antenna radiating into radially inhomogeneous media [15], as illustrated in Figure 8.13. (The treatment of a nonsymmetric excitation requires a vector formulation and will be deferred until Chapter 11.)

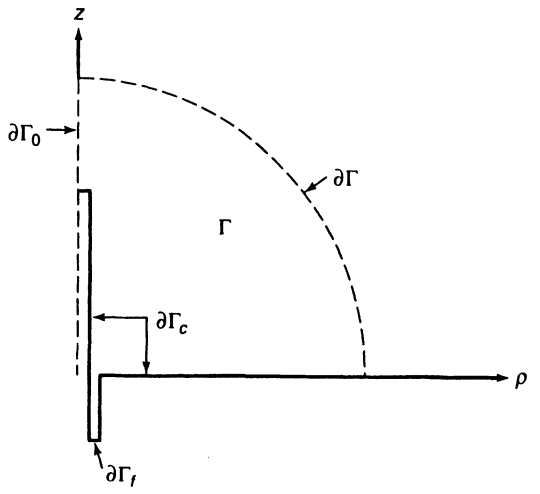

Figure 8.13 Generating sector associated with an axisymmetric monopole antenna geometry.

We will assume that the only nonzero component of the magnetic field is H_ϕ. The ϕ-component of the curl–curl equation

$$\nabla \times \left(\frac{1}{\varepsilon_r} \nabla \times \bar{H} \right) - k^2 \mu_r \bar{H} = 0 \tag{8.138}$$

can be expressed in the form

$$\tilde{\nabla} \cdot \left[\frac{1}{\rho \varepsilon_r} \nabla (\rho H_\phi) \right] + k^2 \frac{\mu_r}{\rho} (\rho H_\phi) = 0 \tag{8.139}$$

where $\tilde{\nabla}$ is the pseudodivergence operator

$$\tilde{\nabla} \cdot \bar{A} = \frac{\partial A_\rho}{\partial \rho} + \frac{\partial A_z}{\partial z} \tag{8.140}$$

A testing function $T(\rho, z)$ can be employed to convert (8.139) into the weak equation

$$\iint_{\Gamma} \frac{1}{\rho\varepsilon_r} \nabla T \cdot \nabla(\rho H_\phi) - k^2 \frac{\mu_r}{\rho} T(\rho H_\phi) = \int_{\partial\Gamma+\partial\Gamma_c+\partial\Gamma_0+\partial\Gamma_f} \frac{1}{\varepsilon_r} T \frac{1}{\rho} \frac{\partial(\rho H_\phi)}{\partial n} \tag{8.141}$$

where $\partial\Gamma$ denotes the radiation boundary, $\partial\Gamma_c$ denotes the surface of any perfectly conducting material that may be present (Figure 8.13), $\partial\Gamma_0$ denotes the $\rho = 0$ axis, and $\partial\Gamma_f$ denotes a feed region (as might be part of a radiating antenna). The form of (8.141) suggests the use of the product ρH_ϕ as the primary unknown rather than H_ϕ alone, and we adopt that approach.

Along perfectly conducting material, the Neumann boundary condition

$$\frac{1}{\rho} \frac{\partial(\rho H_\phi)}{\partial n} = 0 \tag{8.142}$$

must be imposed. In addition, along the $\rho = 0$ axis, the field must satisfy the Dirichlet condition

$$\rho H_\phi = 0 \tag{8.143}$$

Equations (8.142) and (8.143) eliminate the boundary integrals over $\partial\Gamma_c$ and $\partial\Gamma_0$, respectively. We will assume that the radiation boundary $\partial\Gamma$ is circular with radius r and centered at the origin in the ρ–z plane. In addition, we define a local orthogonal coordinate system (n, t) along the boundary so that t is a tangential variable along $\partial\Gamma$. We will impose a second-order local RBC adapted from reference [16], which is derived in Chapter 11. This RBC can be written as

$$\frac{1}{\rho} \frac{\partial(\rho H_\phi^s)}{\partial n} \cong -\frac{jk}{\rho}(\rho H_\phi^s) + \frac{1}{2jk + 2/r} \frac{\partial}{\partial t}\left(\frac{1}{\rho} \frac{\partial}{\partial t}(\rho H_\phi^s)\right) \tag{8.144}$$

If the incident field is exterior to $\partial\Gamma$, Equation (8.144) can be combined with similar expressions involving the incident field and substituted into the weak differential equation to complete the formulation. If the excitation is incorporated via the boundary $\partial\Gamma_f$ depicted in Figure 8.13, it appears as either a nonhomogeneous Dirichlet or Neumann boundary condition and can be incorporated by prescribing field values or by adding the appropriate integral to the right side of (8.141), respectively.

The primary unknown may be expanded in basis functions according to

$$\rho H_\phi(\rho, z) \cong \sum_{n=1}^{N} h_n B_n(\rho, z) \tag{8.145}$$

If identical functions are used for testing, the resulting matrix equation can be written as $\mathbf{Ah} = \mathbf{b}$, where

$$\begin{aligned} A_{mn} = &\iint_{\Gamma} \frac{1}{\rho\varepsilon_r} \nabla B_m \cdot \nabla B_n - k^2 \frac{\mu_r}{\rho} B_m B_n \\ &+ \int_{\partial\Gamma} \frac{jk}{\rho} B_m B_n + \frac{1}{2jk + 2/r} \frac{1}{\rho} \frac{\partial B_m}{\partial t} \frac{\partial B_n}{\partial t} \end{aligned} \tag{8.146}$$

Since the variable ρ appears in the denominator of these expressions, they do not yield to simple closed-form evaluation in terms of the local-area coordinates defined in Chapter 3. However, their evaluation by numerical quadrature is straightforward.

An approach similar to the above formulation has been used to analyze monopole antennas coated with dielectric layers, and the numerical results appear to exhibit excellent agreement with available data [15].

8.9 SUMMARY

This chapter has considered electromagnetic scattering from translationally invariant or rotationally invariant three-dimensional geometries. Usually, these problems can be posed in such a manner as to reduce their computational requirements to those of purely two-dimensional structures. Examples include finite sources radiating in the presence of infinite cylinders and axisymmetric bodies. As might be expected, the price to be paid for the increased computational efficiency is a slight increase in the complexity of the formulation.

REFERENCES

[1] A. F. Peterson and R. Mittra, "Mutual admittance between slots in cylinders of arbitrary shape," *IEEE Trans. Antennas Propagat.*, vol. 37, pp. 858–864, July 1989.

[2] A. D. Yaghjian, "Augmented electric- and magnetic-field equations," *Radio Science*, vol. 16, pp. 987–1001, Nov. 1981.

[3] J. H. Richmond, "A reaction theorem and its application to antenna impedance calculations," *IEEE Trans. Antennas Propagat.*, vol. AP-9, pp. 515–520, Nov. 1961.

[4] S. W. Lee, S. Safavi-Naini, and R. Mittra, "Mutual admittance between slots on a cylinder," Electromagnetics Laboratory Report 77-8, UILU-ENG-77-2549, Dept. of Electrical and Computer Engineering, University of Illinois, Urbana, IL, Mar. 1977.

[5] E. Michielssen, A. F. Peterson, and R. Mittra, "Oblique scattering from inhomogeneous cylinders using a coupled integral equation formulation with triangular cells," *IEEE Trans. Antennas Propagat.*, vol. 39, pp. 485–490, Apr. 1991.

[6] R. G. Rojas, "Scattering by an inhomogeneous dielectric/ferrite cylinder of arbitrary cross-section shape—oblique incidence case," *IEEE Trans. Antennas Propagat.*, vol. AP-36, pp. 238–246, Feb. 1988.

[7] R. B. Wu and C. H. Chen, "Variational reaction formulation of scattering problem for anisotropic dielectric cylinders," *IEEE Trans. Antennas Propagat.*, vol. AP-34, pp. 640–645, May 1986.

[8] A. F. Peterson, "Application of volume discretization methods to oblique scattering from high-contrast penetrable cylinders," *IEEE Trans. Microwave Theory Tech.*, vol. 42, pp. 686–689, Apr. 1994.

[9] A. F. Peterson, S. L. Ray, C. H. Chan, and R. Mittra, "Numerical implementations of the conjugate gradient method and the CG-FFT for electromagnetic scattering," in *Application of Conjugate Gradient Method to Electromagnetics and Signal Analysis (PIER 5)*, ed. T. K. Sarkar, New York: Elsevier, 1991.

[10] M. Abramowitz and I. A. Stegun, *Handbook of Mathematical Functions*, New York: Dover, 1965, p. 591.

[11] M. G. Andreasen, "Scattering from bodies of revolution," *IEEE Trans. Antennas Propagat.*, vol. AP-13, pp. 303–310, Mar. 1965.

[12] J. R. Mautz and R. F. Harrington, "Radiation and scattering from bodies of revolution," *Appl. Sci. Res.*, vol. 20, pp. 405–435, 1969.

[13] A. W. Glisson and D. R. Wilton, "Simple and efficient numerical techniques for treating bodies of revolution," RADC-TR-79-22, Rome Air Development Center, Griffis AFB, NY, March 1979.

[14] S. Govind, D. R. Wilton, and A. W. Glisson, "Scattering from inhomogeneous penetrable bodies of revolution," *IEEE Trans. Antennas Propagat.*, vol. AP-32, pp. 1163–1173, Nov. 1984.

[15] E. Sumbar, F. E. Vermeulen, and F. S. Chute, "Implementation of radiation boundary conditions in the finite element analysis of electromagnetic wave propagation," *IEEE Trans. Microwave Theory Tech.*, vol. 39, pp. 267–273, Feb. 1991.

[16] A. F. Peterson, "Absorbing boundary conditions for the vector wave equation," *Microwave Opt. Technol. Lett.*, vol. 1, pp. 62–64, Apr. 1988.

PROBLEMS

P8.1 Suppose fields $\bar{E}(x, y, z)$ and $\bar{H}(x, y, z)$ are produced by an arbitrary source in free space radiating in the presence of a cylindrical scatterer. A Fourier transformation along z, following (8.1) and (8.2), can be used to replace these fields by $\tilde{\bar{E}}(x, y)e^{jk_z z}$ and $\tilde{\bar{H}}(x, y)e^{jk_z z}$. By combining the $\hat{z}$-component of the appropriate curl–curl equations (1.13) and (1.14) with the associated divergence condition, demonstrate the following:

(a) Assuming that the scatterer is perfectly conducting, show that the equations simplify to

$$\nabla_t^2 \tilde{E}_z + (k^2 - k_z^2)\tilde{E}_z = 0$$
$$\nabla_t^2 \tilde{H}_z + (k^2 - k_z^2)\tilde{H}_z = 0$$

away from the source region, where ∇_t is the transverse gradient defined in Section 8.5. Therefore, in the Fourier transform domain, the three-dimensional problem can be described by an equivalent two-dimensional equation that is a function of the parameter k_z. The TM and TE polarizations are only coupled by the source.

(b) Assuming that the scatterer is a penetrable cylinder described by suitably differentiable functions $\varepsilon_r(x, y)$ and $\mu_r(x, y)$, show that the equations reduce to

$$\nabla_t \cdot \left(\frac{1}{\mu_r}\nabla_t \tilde{E}_z\right) + \frac{k^2\mu_r\varepsilon_r - k_z^2}{\mu_r}\tilde{E}_z = jk_z\nabla_t\left(\frac{1}{\varepsilon_r\mu_r}\right)\cdot\varepsilon_r\tilde{\bar{E}}_t$$
$$\nabla_t \cdot \left(\frac{1}{\varepsilon_r}\nabla_t \tilde{H}_z\right) + \frac{k^2\mu_r\varepsilon_r - k_z^2}{\varepsilon_r}\tilde{H}_z = jk_z\nabla_t\left(\frac{1}{\varepsilon_r\mu_r}\right)\cdot\mu_r\tilde{\bar{H}}_t$$

outside the source region. In fact, these equations also hold if the differentiability of ε_r and μ_r is relaxed to include the case of jump discontinuities in the medium, provided that $\nabla_t((\varepsilon_r\mu_r)^{-1})$ is treated as a generalized function. Therefore, whenever ε_r or μ_r vary with position and $k_z \neq 0$, the transverse and longitudinal fields are coupled and the TM and TE polarizations cannot be treated independently. However, the three-dimensional problem can still be described in the Fourier transform domain by coupled two-dimensional equations that are a function of k_z.

P8.2 Equation (8.10) can be expressed in terms of an inverse discrete Fourier transform, defined in (4.90), and evaluated using an inverse FFT algorithm. Describe the steps necessary to incorporate the FFT and discuss advantages and disadvantages of using the FFT instead of the direct summation of (8.10).

P8.3 Consider a perfectly conducting, circular cylinder with radius a illuminated by an oblique TE wave beyond the visible range of the transform ($k_z^2 > k^2$). Use the eigenfunctions and eigenvalues of the MFIE from Equation (6.5) and the relationship between

the Hankel function and the modified Bessel function of the second kind

$$H_n^{(2)}\left(-j\sqrt{k_z^2-k^2}\rho\right)=\frac{2}{\pi}j^{n+1}K_n\left(\sqrt{k_z^2-k^2}\rho\right)$$

to derive an explicit expression for the eigenvalues of the MFIE when $k_z^2 > k^2$. Show that there are no zeros in the eigenvalue spectrum and thus there is no interior resonance problem when $k_z^2 > k^2$.

P8.4 Derive the TE CFIE describing currents induced on a perfectly conducting cylinder by an obliquely incident plane wave for a range of oblique angles within the visible region of the transform variable ($k_z^2 < k^2$). Develop a method-of-moments discretization using subsectional triangle basis functions and pulse testing functions (see the EFIE approach described in Section 2.4). Provide complete expressions for the matrix entries.

P8.5 Develop an explicit integral expression for the TM bistatic scattering cross section defined in (8.19).

P8.6 Derive component integral equations comprising an augmented MFIE for currents induced on a perfectly conducting cylinder by an obliquely incident TM plane wave within the visible region of the transform variable ($k_z^2 < k^2$). Develop a method-of-moments discretization, providing complete expressions for the matrix entries associated with subsectional pulse basis functions and Dirac delta testing functions.

P8.7 Beginning with Maxwell's equations and assuming an $e^{jk_z z}$-dependence in all field components, derive Equations (8.36) and (8.37).

P8.8 Suppose it is desired to modify the volume integral formulation of Section 8.5 in order to add imbedded perfectly conducting material to the inhomogeneous dielectric cylinder. Derive the generalization of Equations (8.38) and (8.39) that includes the contribution from equivalent electric current on the surface of the imbedded conductor. Leave the result in terms of currents J_z and J_t.

P8.9 Generalize the derivation of the exact eigenfunction RBC from Chapter 3 for the case of oblique incidence and carry out the development to produce Equations (8.67) and (8.68).

P8.10 For obliquely incident waves within the visible region of the transform variable ($k_z^2 < k^2$), a local RBC can be derived by a procedure analogous to that used in Chapter 3 to obtain the Bayliss-Turkel RBC family. Develop first- and second-order RBCs that could be used with the formulation of Section 8.6, assuming a circular boundary of radius a. Leave the result in the form of Equations (8.67) and (8.68). *Hint:* Show that the desired expression for (8.67) can be written in terms of E_z and H_z as follows:

$$\tilde{z}\cdot\tilde{\rho}\times(\nabla\times\tilde{E})\Big|_{(a,\phi,0)}=-\frac{k^2}{k_t^2}\frac{\partial E_z}{\partial\rho}+\frac{\eta k k_z}{k_t^2 a}\frac{\partial H_z}{\partial\phi}$$

after which E_z can be replaced by a Bayliss-Turkel-like condition, to produce (for instance) the second-order RBC

$$\tilde{z}\cdot\tilde{\rho}\times(\nabla\times\tilde{E})|_{(a,\phi,0)}=\frac{k^2}{k_t^2}\left(\frac{\partial E_z^{\text{inc}}}{\partial\rho}-\alpha(a)E_z^{\text{inc}}-\beta(a)\frac{\partial^2 E_z^{\text{inc}}}{\partial\phi^2}\right)$$
$$-\frac{k^2}{k_t^2}\left(\alpha(a)E_z+\beta(a)\frac{\partial^2 E_z}{\partial\phi^2}\right)+\frac{\eta k k_z}{k_t^2 a}\frac{\partial H_z}{\partial\phi}$$

where α and β are defined in Chapter 3. Is it also necessary to replace H_z?

P8.11 Discuss the modifications necessary to extend the differential equation formulation of Section 8.6 to the invisible region of the transform variable ($k_z^2 > k^2$).

P8.12 A hollow linear dipole antenna excited by a ϕ-symmetric feed can be modeled using a specialization of the procedure developed in Section 8.7.

(a) For the ϕ-symmetric case, identify the current components present on the hollow cylinder and specialize the EFIE presented in Equations (8.99) and (8.100) to this case.

(b) Assuming that the linear dipole is discretized into equal-size cells along the axis of the cylinder, simplify the matrix entries given in Equations (8.116)–(8.121) for the ϕ-symmetric case.

(c) A magnetic frill model is often used for the dipole antenna feed. Referring to the frill equations developed in Prob. P1.17, generate an explicit integral expression for the "tested" incident electric field originally defined in (8.111). Discuss the evaluation of any complicating singularities in the integrand.

P8.13 Suppose the hollow cylinder analyzed in Section 8.7 is illuminated with a uniform plane wave incident along the z-axis. How many ϕ-harmonics are necessary to represent this excitation? Develop a procedure for solving the problem that only requires a single matrix solution in this special case.

P8.14 A general three-dimensional local RBC developed for a spherical boundary shape has the form ([16] and Chapter 11)

$$\hat{r} \times (\nabla \times \bar{H}) = jk\bar{H}^{\tan} + \frac{1}{2jk + 2/r} \nabla \times [\hat{r}(\hat{r} \cdot \nabla \times \bar{H})]$$

$$+ \frac{jk}{2jk + 2/r} \nabla^{\tan}(\hat{r} \cdot \bar{H})$$

where $\bar{H}$ refers to the scattered part of the field and $\nabla^{\tan}$ is the tangential part of the gradient, that is, the θ- and ϕ-components. Derive Equation (8.144) by specializing this RBC to the axisymmetric situation described in Section 8.8.